

High-dimensional Bayesian Fourier Analysis For Detecting Circadian Gene Expressions

Silvia Montagna^{*1}, Irina Irincheeva² and Surya T. Tokdar³

¹ESOMAS Department, University of Turin, Turin 10134, Italy

²Clinical Trials Unit (CTU Bern), University of Bern, Bern 3012, Switzerland

³Department of Statistical Science, Duke University, Box 90251, Durham NC 27708, USA

December 15, 2024

Abstract

In genomic applications, there is often interest in identifying genes whose time-course expression trajectories exhibit periodic oscillations with a period of approximately 24 hours. Such genes are usually referred to as “circadian”, and their identification is a crucial step toward discovering physiological processes that are clock-controlled. It is natural to expect that the expression of gene i at time j might depend to some degree on the expression of the other genes measured at the same time. However, widely-used rhythmicity detection techniques do not accommodate for the potential dependence across genes. We develop a Bayesian approach for periodicity identification that explicitly takes into account the complex dependence structure across time-course trajectories in gene expressions. We employ a latent factor representation to accommodate dependence, while representing the true trajectories in the Fourier domain allows for inference on period, phase, and amplitude of the signal. Identification of circadian genes is allowed through a carefully chosen variable selection prior on the Fourier basis coefficients. The methodology is applied to a novel mouse liver circadian dataset. Although motivated by time-course gene expression array data, the proposed approach is applicable to the analysis of dependent functional data at broad.

*simontag@unito.it

Keywords: Bayesian latent factor models, Circadian rhythms, Dependent functional data, Harmonic analysis, Latent threshold methods

1 Introduction

Circadian rhythms are cycles of biological activity based on a 24-hour period which allow organisms to anticipate and adapt to predictable daily oscillations in the environment (Hughes et al. 2010). Circadian rhythms are controlled by the circadian clock, namely a network of mutually interacting proteins that generate transcriptional and translational feedback loops (Jouffe et al. 2013). The molecular mechanisms underlying the circadian clock have been investigated in many organisms (Wichert et al. 2004, Jouffe et al. 2013). In plants, circadian rhythmicity has been extensively studied in the *Arabidopsis thaliana* (Anderson et al. 2006, Edwards et al. 2006, Liverani 2009). In animals, sleep-wake cycles are circadian-regulated to maximize the availability of food as well as to avoid predation. In humans, blood pressure, hormone production, metabolism and other biological cycles are clock-regulated, and disruptions to the circadian rhythms have been linked to a variety of pathologies (Hughes et al. 2010). For example, the International Agency for Research on Cancer reports that “shift-work that involves circadian disruption is probably carcinogenic to humans” (Straif et al. 2007). Consequently, there is a considerable interest in identifying genes that control the timing of many physiological processes.

The identification of clock-genes is performed through examination of their expression levels or “transcripts”. With regard to the functioning of a cell, deoxyribonucleic acid (DNA) is first duplicated into messenger ribonucleic acid (mRNA), and the RNA is then used for protein synthesis. To quantify the expression of a specific gene, it is possible to measure the concentration of RNA molecules associated with this gene. By using this principle, microarray analysis allows investigators to measure many hundreds or thousands of transcripts simultaneously, and then statistical methods are needed to detect periodic pathways among a very high number of gene expression profiles.

Several authors have proposed methods for periodicity identification in biomedical research over the last couple of decades. Chudova et al. (2009) give an excellent review of the main existing techniques, which can be broadly classified as time domain or frequency domain analyses. Time domain methods are pattern-matching techniques: cosine curves of varying periods and phases are fit to each expression profile separately, and the best fit to the experimental data is retained to

describe the signal (Straume 2004, Hughes et al. 2010). Pattern-matching methods are simple and computationally efficient, but not very effective at finding periodic signals that are not perfectly sinusoidal (Chudova et al. 2009). Frequency domain approaches combine spectral analysis with multiple hypothesis testing (Wichert et al. 2004, Ahdesmäki et al. 2005). Specifically, one obtains the spectrum of a transcript and the hypothesis of significance of the dominant frequency is tested against the null hypothesis of absence of periodic signal. The analysis is carried out probe by probe independently, and the obtained significance values are then corrected for multiplicity. Chudova et al. (2009) remark that frequency domain methods are most effective on long time series. However, this is not a typical feature of circadian studies, which are usually designed to collect data every 2 or 4 hours over two circadian cycles. Therefore, coarse sampling and short periods of data collection are typical features of these studies. Also, the authors claim that existing computational methods are biased toward discovering genes whose transcripts follow sine-wave patterns. Chudova et al. (2009) propose an analysis of variance periodicity detector and its Bayesian extension for the identification of patterns of arbitrary shape. Costa et al. (2013) propose a methodology based on spectrum resampling (SR). SR is a technique based around an iterative bootstrapping of a smoothed power series to provide a steady-state model which reflects the data. The authors point out that SR is especially designed to be robust to non-sinusoidal and noisy cycles.

As a separate line of research for the analysis of genomic data, several model-based clustering algorithms have been proposed in both the classical and Bayesian framework (Yeung et al. 2001, Luan & Li 2003, Wakefield et al. 2003). However, clustering algorithms should be customized to reflect the scientific interest. In particular, efforts should concentrate around refining clusters that contain potentially interesting genes while no time should be spent on finding an optimal partition of obviously non-circadian genes. In this regard, Anderson et al. (2006) use the algorithm in Heard et al. (2006) many times on various partitions of the transcripts, with a Fourier basis to extract rhythmically expressed genes. A score is calculated for each partition of the genes and the score determines the clustering.

A key assumption in all the approaches above is that of independence across transcripts. The clustering algorithm described in Anderson et al. (2006) assumes dependence at a cluster level only whereas clusters vary independently. Although practical from a computational perspective, the independence assumption is often too strong to be realistic in many applications, including

the data set that motivates our work. In particular, Jouffe et al. (2013) design a microarray experiment to assess whether the circadian clock coordinates mRNA translation in mouse liver. Male mice between 10 and 12 weeks of age were kept under standard animal housing conditions, with free access to food and water and in 12 hours light/12 hours dark cycles. However, animals were fed only at night during 4 days before the experiment to reduce the effects of feeding rhythm. 3 μg of liver polysomal and total RNAs were extracted independently from two mice sacrificed every 2 hours during 48 hours, and used for the synthesis of biontynylated cytosine RNA according to Affymetrix protocol. The resulting fluorescence signal was analysed with Affymetrix software (refer to Jouffe et al. (2013) for an extensive description of the experiment). Data are deposited on the Gene Expression Omnibus database under the reference GSE33726. Figure A shows examples of temporal expression profiles of a subset of genes from the dataset. Being collected on different mice, the measurements across time can reasonably be assumed to be independent. However, it is natural to expect that the expression of gene i at time j might depend to some degree on the expression of the other genes measured at the same time. Therefore, the dependence across expression trajectories should be modelled and explicitly accounted for.

[Figure 1 about here.]

In this paper, we propose a flexible Bayesian approach that identifies periodic signals in gene expression profiles while accounting for dependence in the functional data. Specifically, we decompose the true, de-noised underlying signal for each transcript as a series expansion of sine and cosine waves to extract rhythmic signals, while we also accommodate for local deviations from these smooth, sinusoidal trajectories. Furthermore, we accommodate conditional dependence across probes at each time point through a latent factor framework. Dimensionality reduction and sparsity are induced through careful modeling of the latent factors as well as the local and Fourier basis coefficients. The proposed approach gives a comprehensive description of cyclic rhythms through posterior summaries of the model parameters. The proposed approach is tested on the mouse liver mRNA dataset of Jouffe et al. (2013) and on simulation experiments.

The rest of the paper is organized as follows. Section 2 presents our dependent latent factor approach. Section 3 discusses the choice of prior distributions for the model parameters, and Section 4 outlines the posterior computation. In Section 5 we apply our approach to synthetic datasets. Section 6 present the application of our methodology to the mouse liver mRNA dataset.

Concluding remarks are presented in Section 7. Finally, the Appendix presents the analysis of an additional circadian dataset.

2 Methodology

2.1 Overview

We consider data from a gene expression experiment in the form of a $p \times T$ matrix $\mathbf{Y} = \{y_{ij}\}$, where entry y_{ij} denotes the observed mRNA concentration for gene i at time t_j , for $i = 1, \dots, p$, and with p denoting the total number of genes. In circadian microarray studies, data are typically collected over two complete circadian cycles and the sampling rate is usually either two or four hours. In our motivating application (Jouffe et al. 2013), the sampling rate is two hours, thus $t_j = 0, 2, 4, \dots, 46$ and $T = 24$. Hereafter, we will make explicit reference to the study in Jouffe et al. (2013), although the structure applies more generally to any circadian microarray experiment with the appropriate choices of T and sampling rate. We assume that the y_{ij} 's are error-prone measurements of an underlying smooth true trajectory

$$y_{ij} = f_i(t_j) + \nu_{ij}. \quad (1)$$

Suppose that the de-trended and centered true signal for gene i at time t_j , $f_i(t_j)$, can be decomposed as

$$f_i(t_j) = \sum_{m=1}^q (\theta_{i,2m-1} b_{2m-1}(t_j) + \theta_{i,2m} b_{2m}(t_j)) = \boldsymbol{\theta}_{i,m}^\top \mathbf{b}_m(t_j) = \boldsymbol{\theta}_{i,m}^\top \mathbf{b}_{m,j},$$

where for $m = 1, \dots, q$ we define $\boldsymbol{\theta}_{i,m} = (\theta_{i,2m-1}, \theta_{i,2m})^\top$ and $\mathbf{b}_{m,j} = [b_{2m-1}(t_j), b_{2m}(t_j)]^\top$. The vector

$$\mathbf{b}_j = [b_1(t_j), b_2(t_j), \dots, b_{2q-1}(t_j), b_{2q}(t_j)]^\top$$

represents a set of $2q$ fixed basis functions evaluated at time t_j . One popular basis for a space of periodic functions is the Fourier basis

$$\mathbf{b}(t) = \left[\sin\left(\frac{2\pi}{\omega_1} t\right), \cos\left(\frac{2\pi}{\omega_1} t\right), \dots, \sin\left(\frac{2\pi}{\omega_q} t\right), \cos\left(\frac{2\pi}{\omega_q} t\right) \right],$$

where $\{\omega_m\}_{m=1}^q$ denotes the periodicity of the signal and t is time represented by a unit-interval increase. The q period lengths w_m are assumed known and fixed. Since there are 24 time points per transcript in the mouse liver ribosomal proteins dataset, we can use up to twelve sine/cosine pairs of harmonics. According to Nyquist-Shannon theorem and common sense, the possible range of periods would be 4, 6, 8, 10, 12, 14, 16, 18, 20, 22 or 24 hours, but biologists would argue to reduce this list to 4, 6, 8, 12 or 24 hours only. In practice, suitable period lengths can be proposed by inspecting the average periodogram of the probes and choosing the frequencies of the q ordered largest peaks in the spectrum. Here w_1 is the shortest period, and w_2, \dots, w_q correspond to longer periods.

The term ν_{ij} in Equation 1 models the deviation between the observed measurement at time t_j , y_{ij} , and the underlying smooth profile. In the original study (Jouffe et al. 2013), two mice are sacrificed every two hours and the reported p expression levels at time j are obtained by pooling 3 μg of total mRNA from each mice. Therefore, the ν_{ij} 's are correlated across probes, i . Specifically, each profile at time j may deviate from its own underlying truth because of a ‘‘mouse effect’’ which could make, e.g. a certain protein more expressed than the corresponding truth and another protein less expressed at time j . To accommodate dependence across probes at time j we adopt a sparse factor model:

$$\boldsymbol{\nu}_j = \mathbf{\Lambda}\boldsymbol{\eta}_j + \boldsymbol{\epsilon}_j, \quad (2)$$

with $\boldsymbol{\nu}_j = [\nu_{1j}, \dots, \nu_{pj}]^\top$, $\mathbf{\Lambda} = [\boldsymbol{\lambda}_1, \dots, \boldsymbol{\lambda}_p]^\top$ is a $p \times k$ factor loading matrix with elements $\{\lambda_{ih}\}_{i=1, \dots, p; h=1, \dots, k}$, $\boldsymbol{\eta}_j = (\eta_{1j}, \dots, \eta_{kj})^\top$ is $k \times 1$ vector of latent factors at time j which explains mice-specific deviations of the expression levels at time j from their corresponding truth (it explains why proteins at time j may be systematically over- or under-expressed with respect to the ‘‘truth’’), and $\boldsymbol{\epsilon}_j$ is a residual error. Sparsity here is necessary given the very large p , and Section 3 discusses how sparsity can be achieved through the modeling of $\mathbf{\Lambda}$.

The full model for subject i at time t_j is

$$\begin{aligned} y_{ij} &= g_i(t_j) + \boldsymbol{\lambda}_i^\top \boldsymbol{\eta}_j + \epsilon_{ij}, \quad \text{with } \epsilon_{ij} \sim N(0, \sigma_i^2), \\ g_i(t_j) &= f_i(t_j) + \mathbf{c}_j^\top \boldsymbol{\gamma}_i = \mathbf{b}_j^\top \boldsymbol{\theta}_i + \mathbf{c}_j^\top \boldsymbol{\gamma}_i, \end{aligned} \quad (3)$$

where the first term $\mathbf{b}_j^\top \boldsymbol{\theta}_i = \mathbf{b}(t_j)^\top \boldsymbol{\theta}_i$ captures periodic oscillations, the second term $\mathbf{c}_j^\top \boldsymbol{\gamma}_i = \mathbf{c}(t_j)^\top \boldsymbol{\gamma}_i$ captures local deviations from the underlying periodic oscillation (if present), and the

third term $\boldsymbol{\lambda}_i^\top \boldsymbol{\eta}_j$ captures across-proteins dependence (if present). The importance of the $\mathbf{c}_j^\top \boldsymbol{\gamma}_i$ component becomes evident in studies where mice are given a stimulus at the beginning of the experiment. The stimulus might produce deviations of the observed expression levels from the true signals, and these deviations shall manifest at different times across proteins and last for a different amount of time, if present at all. After standardizing the time domain to $[0, 1]$, suitable choices for $\mathbf{c}(t_j)^\top$ are Gaussian kernels

$$c_l(t_j) = \exp\{-\psi\|t_j - \xi_l\|^2\}, \quad l = 1, \dots, \tilde{T} \quad (4)$$

with equally spaced kernel location $\xi_1, \dots, \xi_{\tilde{T}}$ and bandwidth parameter ψ , or B-splines basis functions. $\boldsymbol{\theta}_i$ ($\boldsymbol{\gamma}_i$) is the $2q \times 1$ ($\tilde{T} \times 1$) vector of fixed periodic (local) basis function coefficients for protein i . Greater \tilde{T} corresponds to more flexibility in modeling local deviations. We follow standard practice in normalizing the data prior to analysis and hence do not include an intercept term in (3). We use $\mathbf{y}_i = (y_{i1}, \dots, y_{iT})^\top$ to denote the i -th row of \mathbf{Y} (the i -th protein observed at times $1, \dots, T$); and $\mathbf{y}^{(j)} = (y_{1j}, \dots, y_{pj})^\top$ to denote the j -th column of \mathbf{Y} (p proteins observed at the time j). Construction (3) for y_{ij} can now be rewritten in vector notation as

$$\mathbf{y}_i = \mathbf{B}\boldsymbol{\theta}_i + \mathbf{C}\boldsymbol{\gamma}_i + \boldsymbol{\nu}_i = \mathbf{B}\boldsymbol{\theta}_i + \mathbf{C}\boldsymbol{\gamma}_i + \boldsymbol{\eta}\boldsymbol{\lambda}_i + \boldsymbol{\varepsilon}_i, \quad (5)$$

where

$$\mathbf{B} = \begin{bmatrix} \mathbf{b}_1^\top \\ \vdots \\ \mathbf{b}_T^\top \end{bmatrix} \in \mathfrak{R}^{T \times 2q}; \quad \mathbf{C} = \begin{bmatrix} \mathbf{c}_1^\top \\ \vdots \\ \mathbf{c}_T^\top \end{bmatrix} \in \mathfrak{R}^{T \times \tilde{T}}; \quad \boldsymbol{\lambda}_i \in \mathfrak{R}^k; \quad \boldsymbol{\eta} = \begin{bmatrix} \boldsymbol{\eta}_1^\top \\ \vdots \\ \boldsymbol{\eta}_T^\top \end{bmatrix} \in \mathfrak{R}^{T \times k};$$

$$\boldsymbol{\varepsilon}_i = (\varepsilon_{i1}, \dots, \varepsilon_{iT})^\top \sim N_T(\mathbf{0}, \sigma_i^2 \mathbf{I}_T) \text{ with } T \times T \text{ identity matrix } \mathbf{I}_T;$$

or

$$\mathbf{y}^{(j)} = \boldsymbol{\Theta}\mathbf{b}_j + \boldsymbol{\Gamma}\mathbf{c}_j + \boldsymbol{\nu}^{(j)} = \boldsymbol{\Theta}\mathbf{b}_j + \boldsymbol{\Gamma}\mathbf{c}_j + \boldsymbol{\Lambda}\boldsymbol{\eta}_j + \boldsymbol{\varepsilon}^{(j)}, \quad (6)$$

where

$$\boldsymbol{\Theta} = \begin{bmatrix} \boldsymbol{\theta}_1^\top \\ \vdots \\ \boldsymbol{\theta}_p^\top \end{bmatrix} \in \mathfrak{R}^{p \times 2q}; \quad \boldsymbol{\Gamma} = \begin{bmatrix} \boldsymbol{\gamma}_1^\top \\ \vdots \\ \boldsymbol{\gamma}_p^\top \end{bmatrix} \in \mathfrak{R}^{p \times \tilde{T}}; \quad \boldsymbol{\Lambda} = \begin{bmatrix} \boldsymbol{\lambda}_1^\top \\ \vdots \\ \boldsymbol{\lambda}_p^\top \end{bmatrix} \in \mathfrak{R}^{p \times k};$$

$$\boldsymbol{\varepsilon}^{(j)} = (\varepsilon_{1j}, \dots, \varepsilon_{pj})^\top \sim N_p(\mathbf{0}, \boldsymbol{\Sigma}), \quad \boldsymbol{\Sigma} = \text{diag}\{\sigma_1^2, \dots, \sigma_p^2\}$$

The latent factors $\boldsymbol{\eta}_j$ have a natural interpretation as (mice-specific) unobserved traits of the two mice sacrificed at time j that explain the dependence structure across proteins at time t_j . Hereafter we follow standard practice and assign a normal prior to the latent factors at time t_j , $\boldsymbol{\eta}_j \sim N(\mathbf{0}, \mathbf{I}_k)$. Proteins are assumed to be independent given the latent factors, and dependence among proteins is induced by marginalizing over the distribution of the factors, so marginally $\mathbf{y}^{(j)} \sim N(\boldsymbol{\Theta}\mathbf{b}_j + \boldsymbol{\Gamma}\mathbf{c}_j, \boldsymbol{\Lambda}\boldsymbol{\Lambda}^\top + \boldsymbol{\Sigma})$. In practical applications involving moderate to large p , the number of factors k is typically much smaller than p , thus inducing a sparse characterization of the unknown covariance matrix $\boldsymbol{\Lambda}\boldsymbol{\Lambda}^\top + \boldsymbol{\Sigma}$.

The next Section discusses suitable prior choices for the model parameters in Equations (5)-(6) and examines how these choices translate into the ability to perform period identification.

3 Prior elicitation

With regard to the modeling of the basis coefficients $\{\boldsymbol{\theta}_i, \boldsymbol{\gamma}_i\}_{i=1}^p$, we need a technical device to induce sparsity / parsimony, hence avoid over-fitting, whilst retaining an easy interpretation of the method. The latter is particularly crucial for the modeling of $\boldsymbol{\theta}_i$ since inference on this set of parameters is the primary interest of our work. Although different formulations are possible, we adopt the latent threshold model (LTM) of Nakajima & West (2013). The LTM is a direct extension of standard Bayesian variable selection which assigns non-zero prior probabilities to zero values of regression parameters, and continuous priors centered at zero otherwise.

We begin introducing the LTM for the elements of $\boldsymbol{\gamma}_i$. Denote with γ_{il} the l th component of the $\tilde{T} \times 1$ vector of local basis coefficients $\boldsymbol{\gamma}_i$. The model assumes

$$\gamma_{i,l} = \tilde{\gamma}_{i,l} \mathbb{1}(|\tilde{\gamma}_{i,l}| \geq \varpi_{i,l}^*), \quad (7)$$

where $\varpi_{i,l}^* \geq 0$ is a latent threshold and $\mathbb{1}(\cdot)$ denotes the indicator function. Equation (7) embodies sparsity/shrinkage and parameter reduction when necessary, with the l th local basis coefficient shrunk to zero when it falls below a threshold. If the true smooth profile for protein i is given by the oscillatory behavior measured by $\mathbf{B}\boldsymbol{\theta}_i$ with no time localized deviations, then each component of vector $\tilde{\boldsymbol{\gamma}}_i = \{\tilde{\gamma}_{i,l}\}_{l=1}^{\tilde{T}}$ is expected to be uniquely shrunk to zero. Non-zero components allow for time-localized deviations. The vector $\tilde{\boldsymbol{\gamma}}_i$ is modeled as

$$\tilde{\boldsymbol{\gamma}}_i = \mathbf{Z}\boldsymbol{\lambda}_i + \boldsymbol{\alpha}_i^\gamma \quad \text{and} \quad \boldsymbol{\alpha}_i^\gamma \sim N_{\tilde{T}}(\mathbf{0}, \mathbf{I}), \quad (8)$$

where \mathbf{Z} is a $\tilde{T} \times k$ matrix and $\boldsymbol{\lambda}_i$ is the vector of factor loadings for protein i as in (3). We assign a (multivariate) standard normal prior to the rows of \mathbf{Z} , $\mathbf{Z}_j^\top \sim N_k(\mathbf{0}, \mathbf{I})$, $j = 1, \dots, \tilde{T}$.

We adopt the same variable selection prior for the periodic basis coefficients. Denote with $\boldsymbol{\theta}_{im} = \{\theta_{i,2m-1}, \theta_{i,2m}\}^\top$ the vector of $2m - 1$ th and $2m$ th components of $\boldsymbol{\theta}_i$, $m = 1, \dots, q$. Thus, $\theta_{i,2m-1}$ is the coefficient of the $2m - 1$ th sine basis and $\theta_{i,2m}$ is the coefficient of the $2m$ th cosine basis, both harmonics of period w_m . To enhance a correct interpretation of periodicity, we need to switch off $\theta_{i,2m-1}$ and $\theta_{i,2m}$ jointly provided that shrinkage is supported by the data. Therefore, we assume:

$$\boldsymbol{\theta}_{i,m} = \tilde{\boldsymbol{\theta}}_{i,m} \mathbb{1}(\|\tilde{\boldsymbol{\theta}}_{i,m}\| \geq \varpi_{i,m}), \quad (9)$$

where $\varpi_{i,m}$ is a latent threshold. The idea behind (9) is that the value of the w_m -periodic basis coefficients is shrunk to zero when their norm falls below a m th- (and protein-) specific threshold. Suppose, for example, that the set of probable periods is $\{4, 6, 8, 12, 24\}$ hours, i.e. $q = 5$. If the i th time series $\mathbf{y}_i = (y_{i1}, \dots, y_{iT})^\top$ is generated with a true signal $f(t) = A \sin(\frac{2\pi}{12}t + \varphi)$, which is a 12 hours periodic function with phase φ hours and amplitude A , then column i of $\boldsymbol{\Theta}$ is expected to contain only two non-zero elements, $\theta_{i,7}$ and $\theta_{i,8}$, for representing sum of 12-hour periodic basis functions $b_7 = \sin(\frac{2\pi}{12}t)$, $b_8 = \cos(\frac{2\pi}{12}t)$. There are two possibilities of parametrization for $\theta_{i,7}$ and $\theta_{i,8}$: first $\theta_{i,7} = A \sin(\varphi)$, $\theta_{i,8} = A \cos(\varphi)$; and second $\theta_{i,7} = A \cos(\varphi)$, $\theta_{i,8} = A \sin(\varphi)$. Clearly, this lack of identifiability in $\boldsymbol{\theta}_{i,4}$ does not affect inference for phase and amplitude.

Further, we assume $\tilde{\boldsymbol{\theta}}_i = \{\tilde{\boldsymbol{\theta}}_{i,m}\}_{m=1}^q$ is modeled as

$$\tilde{\boldsymbol{\theta}}_i = \mathbf{W}\boldsymbol{\lambda}_i + \boldsymbol{\alpha}_i^\theta \quad \text{and} \quad \boldsymbol{\alpha}_i^\theta \sim N_{2q}(\mathbf{0}, \mathbf{I}), \quad (10)$$

where \mathbf{W} is a $2q \times k$ matrix and $\boldsymbol{\lambda}_i$ is the vector of factor loadings for protein i . Similar to the structure on \mathbf{Z} , we assume $\mathbf{W}_j^\top \sim N_k(\mathbf{0}, \mathbf{I})$, $j = 1, \dots, 2q$. This simple structure on $\boldsymbol{\gamma}_i$ and $\boldsymbol{\theta}_{i,m}$ in (7)-(9) allows to flexibly take into account the dependence among parameters $\boldsymbol{\gamma}_i$, $\boldsymbol{\theta}_{i,m}$ and $\boldsymbol{\lambda}_i$.

To continue, we adopt a multiplicative gamma process shrinkage prior (MGPSPP) on the loadings

$$\begin{aligned} \lambda_{ih} | \phi_{ih}, \tau_h &\sim N(0, \phi_{ih}^{-1} \tau_h^{-1}), \quad \phi_{ih} \sim \text{Ga}\left(\frac{\rho}{2}, \frac{\rho}{2}\right), \quad \tau_h = \prod_{l=1}^h \zeta_l \\ \zeta_1 &\sim \text{Ga}(a_1, 1), \quad \zeta_l \sim \text{Ga}(a_2, 1), \quad l \geq 2, \quad i = 1, \dots, p, \end{aligned}$$

with $h = 1, \dots, k$, the number of latent factors. τ_h is a global shrinkage parameter for the h -th column, and ϕ_{ih} is a local shrinkage parameter for the elements in the h -th column. In matrix

notation, row i of $\mathbf{\Lambda}$ has prior

$$\boldsymbol{\lambda}_i^\top | \{\phi_{ih}\}_{h=1}^k, \{\tau_h\}_{h=1}^k \sim N_k(\mathbf{0}, \mathbf{D}_i), \quad (11)$$

with $\mathbf{D}_i = \text{diag}(\phi_{i1}^{-1}\tau_1^{-1}, \dots, \phi_{ik}^{-1}\tau_k^{-1})$. This prior favors more shrinkage as the column index of $\mathbf{\Lambda}$ increases, thus avoids factor splitting by concentrating more and more shrunk loadings in the last columns of $\mathbf{\Lambda}$. The MGSPS was originally proposed by Bhattacharya & Dunson (2011) for sparse modeling of high-dimensional covariance matrices. The authors embedded the MGSPS into an adaptive Gibbs sampler which allowed for block update of the rows of the $\mathbf{\Lambda}$ while accounting for an adaptive choice of the number of factors, k . The main idea consisted of monitoring the columns $\mathbf{\Lambda}$ whose loadings were all within some pre-specified neighborhood of zero. If the number of such columns dropped to zero, one extra column was added to $\mathbf{\Lambda}$ and otherwise the redundant columns were discarded. We adopt here the same adaptive block Gibbs sampler to retain only important factors and reduce computing time as a side. Additional details on this prior and the adaptive algorithm can be found in Bhattacharya & Dunson (2011).

To conclude the model formulation, we need to specify prior distributions on the latent threshold parameters. The straightforward extension of Nakajima & West (2013) to our scenario leads to a dependent prior for $\varpi_{i,m}$ (and $\varpi_{i,l}^*$) of the type $\varpi_{i,m} \sim \text{Unif}(0, U_{i,m})$ for $i = 1, \dots, p$ and $m = 1, \dots, q$, where the upper bound of the uniform prior is function (thus dependent) of other model parameters. Nakajima & West (2013) give a thorough discussion on the choice of the upper bound $U_{i,m}$ and its impact on the sparsity structure of the model. We recognize, however, that a dependent prior on the latent thresholds would lead to unnecessary complications in the posterior update of some model parameters within our construction. Therefore, we opt for independent priors on the latent thresholds

$$\varpi_{i,m} \sim \text{Unif}(0, K_\theta), \quad i = 1, \dots, p, \text{ and } m = 1, \dots, m \quad (12)$$

$$\varpi_{i,l}^* \sim \text{Unif}(0, K_\gamma), \quad i = 1, \dots, p, \text{ and } l = 1, \dots, \tilde{T} \quad (13)$$

$$K_\theta \sim \text{Pareto}(a_\theta, b_\theta), \quad (14)$$

$$K_\gamma \sim \text{Pareto}(a_\gamma, b_\gamma). \quad (15)$$

K_θ and K_γ are fundamental sparsity parameters shared across subjects. Smaller or larger degrees of expected sparsity might be needed depending on the context, thus these parameters need to be

inferred from the data. In general, the smaller these parameters are estimated to be the less sparse the model becomes. Clearly, there is no inherent interest in direct inference on the thresholds themselves; the interest is their roles as defining the ability to shrink parameters when the data support sparsity. Correspondingly, there is no interest in the underlying values of the latent $\tilde{\gamma}_i$ and $\tilde{\theta}_i$ when below threshold.

In addition to sparsity, K_θ and K_γ play an important role in controlling for multiplicity adjustments. When analyzing microarray expression data, tens of thousands of genes are estimated simultaneously, so the problem of multiple testing must be considered. (Müller et al. 2006) remark that posterior inference adjusts for multiplicities, and no further adjustment is required, provided that the probability model includes a positive prior probability of non-periodic expression for each protein i , and a hyperparameter that defines the prior probability mass for non-periodic expression. In our context, the two conditions are controlled and satisfied by treating K_θ and K_γ as model parameters with hyperpriors as in (14)-(15). A discussion on the role and specification of hyperparameters $a_\theta, b_\theta, a_\gamma, b_\gamma$ is deferred to the next Section.

3.1 Prior sparsity probabilities

The hyperparameters in Equations (14)-(15) have a key role in defining the prior (and posterior) probability of shrinkage of the periodic and local basis coefficients. Depending on the data and context, different degrees of sparsity might be desired, thus requiring careful tuning of these parameters. For simplicity, we focus here on the impact that different choices of a_γ and b_γ have on the prior probability of shrinkage of the local basis coefficients $\gamma_{i,l}$'s.

With no loss of generality, assume $\mathbf{Z}_l^\top \boldsymbol{\lambda}_i = 0$ so that $\tilde{\gamma}_{i,l} \mid \mathbf{Z}_l, \boldsymbol{\lambda}_i \sim N(0, 1)$. Conditional on the latent thresholds, one can easily derive the probability that coefficient $\gamma_{i,l}$ is not switched off as

$$P(\gamma_{i,l} \neq 0 \mid \varpi_{i,l}^*) = 2\{1 - \Phi(\varpi_{i,l}^*)\}, \quad (16)$$

where $\Phi(\cdot)$ denotes the standard normal cumulative density function. By marginalizing over the prior distribution of the thresholds, we obtain

$$p_\gamma := P(\gamma_{i,l} \neq 0 \mid K_\gamma) = \int_0^{K_\gamma} 2\{1 - \Phi(\varpi_{i,l}^*)\} \times \frac{1}{K_\gamma} d\varpi_{i,l}^*, \quad (17)$$

which corresponds to the prior probability of non-shrinkage conditional on K_γ . Note that p_γ is neither protein-dependent (i) nor basis-dependent (l). Integral (17) is not available in closed form, but can be evaluated via numerical integration. If we denote with $\gamma_{i,l}^*$ the indicator for the decision of not shrinking parameter $\gamma_{i,l}$, then the $\gamma_{i,l}^*$'s are independent and identically distributed (*i.i.d.*) random variables with common probability of success p_γ ,

$$\gamma_{i,l}^* := \mathbb{1}(\gamma_{i,l} \neq 0) \mid p_\gamma \stackrel{i.i.d.}{\sim} \text{Bernoulli}(p_\gamma). \quad (18)$$

Though separate decisions of shrinkage are to be taken on each parameter $\gamma_{i,l}$, the different cases are treated in unison within a framework of exchangeability.

To evaluate the dependence of p_γ to hyperparameters a_γ and b_γ , we generated independent realizations of K_γ from the prior distribution (15) given a particular choice of a_γ and b_γ . For each of these realizations, we evaluated integral (17) and constructed the histogram of the so-obtained p_γ 's. Figure 2 shows the distribution of p_γ for different choices of a_γ and b_γ , with b_γ varying along the rows and a_γ along the columns. It emerges clearly that b_γ defines an upper bound on the prior probability of non-shrinkage. Larger choices of b_γ determine a smaller upper bound on p_γ (the upper bound of the x -axis decreases by moving along the rows), thus effectively favoring a more sparse structure. For any given value of b_γ , small (large) values of a_γ tend to favor smaller (larger) p_γ whereas for $a_\gamma \approx 1$ the prior distribution of p_γ becomes

$$p_\gamma \stackrel{approx}{\sim} \text{Uniform}(0, U_{p_\gamma}), \quad (19)$$

where U_{p_γ} is the upper bound on the distribution of p_γ . This result is true for larger choices of b_γ in particular.

[Figure 2 about here.]

A context where we expect high sparsity with, say, 90% thresholding implies a fairly high choice of b_γ , and a value of $b_\gamma = 10$ or above leads to a marginal sparsity probability exceeding 0.92. Unless the context involves substantive information to suggest favoring smaller or larger degrees of expected sparsity, an approximately uniform prior with $a_\gamma = 1$ and $b_\gamma = 5$ or 10 is a good default for p_γ . A similar reasoning follows for p_θ .

3.2 Period detection

The LTM on the periodic basis coefficients eases the identification of those proteins that are more likely to be periodically expressed. Denote with TS the total number of thinned posterior samples post-burn-in obtained by running a Markov-Chain-Monte-Carlo (MCMC) algorithm to update the model parameters, i.e. $TS = \frac{\text{Tot. \# runs} - \text{burn-in}}{\text{thin}}$ (see Section 4 for details). We can easily derive the posterior probability of any simple periodicity (4, 6, 8 hours, etc.) by counting the proportion of posterior samples for which $\{\theta_{i,2m-1}, \theta_{i,2m}\}$ are *not* shrunk to zero while the remaining θ_s 's are switched off. For example, the posterior probability that protein i is circadian can be computed as

$$P(\text{Protein } i \text{ is circadian}) = \frac{1}{TS} \sum_{g=1}^{TS} \mathbb{1}(\{\theta_{i,l}^{(g)}\}_{l=1}^{2q-2} \equiv \mathbf{0} \text{ and } \{\theta_{i,2q-1}^{(g)}, \theta_{i,2q}^{(g)}\} \neq \mathbf{0}) \quad (20)$$

If we were interested in quantifying the probability of a protein being periodically expressed without making any specific reference to its period, we could simply count the proportion of posterior samples for which any pair $\{\theta_{i,2m-1}, \theta_{i,2m}\}$ is *not* shrunk whereas the remaining parameters are switched off. In symbols,

$$P(\text{Protein } i \text{ is periodic}) = \frac{1}{TS} \sum_{g=1}^{TS} \mathbb{1} \left\{ \begin{array}{l} [(\theta_{i,1}^{(g)}, \theta_{i,2}^{(g)}) \neq \mathbf{0} \text{ and } (\theta_{i,l}^{(g)})_{l=3}^q \equiv \mathbf{0}] \text{ or} \\ [(\theta_{i,3}^{(g)}, \theta_{i,4}^{(g)}) \neq \mathbf{0} \text{ and } (\theta_{i,l}^{(g)})_{l \in \{1,2,4,\dots,q\}} \equiv \mathbf{0}] \text{ or} \\ \vdots \\ [(\theta_{i,l}^{(g)})_{l=1}^{2q-2} \equiv \mathbf{0} \text{ and } (\theta_{i,2q-1}^{(g)}, \theta_{i,2q}^{(g)}) \neq \mathbf{0}] \end{array} \right\} \quad (21)$$

Biologists are interested in identifying clock proteins without incurring into too many false discoveries. Then, we need to compile a list of proteins for which the hypothesis of 24 hours periodicity is probably true, and we want the list to be as large as possible while bounding the rate of false discoveries by some threshold, say k^* . We can rank the proteins according to increasing values of $\beta_i = 1 - \Pr(\text{Protein } i \text{ is circadian})$ and declare all proteins with β_i below a threshold, κ , as clock-controlled proteins

$$\beta_i^* = \mathbb{1}(\beta_i \leq \kappa), \quad (22)$$

where β_i^* is an indicator for the decision to report protein i as circadian. (Müller et al. 2004) show that (22) is the optimal decision rule under several loss functions that combine false negative and false discovery counts and/or rates, and the choice of the loss function determines the specific value of κ . In addition, the authors show that the result is true for any probability model with non-zero

prior probability for periodic and non-periodic expression. In particular, the probability model can include dependence across proteins.

Given the data, the expected number of false discoveries is

$$C(\kappa) = \sum_i \beta_i \mathbb{1}[\beta_i \leq \kappa]$$

since β_i is the conditional probability that identifying protein i as circadian creates a type I error. Hereafter we follow Newton et al. (2004) and choose a data-dependent $\kappa \leq 1$ as large as possible such that $C(\kappa)/|J| \leq k^*$, where $|J| > 0$ is the size of the list. So, $C(\kappa)/|J|$ is the expected rate of false discoveries given the data.

3.3 Inference on phase and amplitude

In addition to period estimation, phase and amplitude of rhythmic transcripts must be accurately estimated. Grouping rhythmic transcripts by phase may suggest a common underlying regulatory mechanism. Also, the most robust cyclic proteins can be identified by amplitude. By making use of standard results from Fourier analysis, any simply periodic function $A \cos(\frac{2\pi}{w}t - \psi)$ can be expressed in an essentially unique manner as

$$A \cos\left(\frac{2\pi}{w}t - \psi\right) = A_1 \sin\left(\frac{2\pi}{w}t\right) + A_2 \cos\left(\frac{2\pi}{w}t\right)$$

The function above is said to have amplitude A and phase shift ψ . Therefore, the de-trended and centered true signal for protein i at time t_j can be written as

$$f_i(t_j) = \sum_{m=1}^q A_{i,m} \cos\left(\frac{2\pi}{w_m}t_j - \psi_{i,m}\right) \quad (23)$$

$$= \sum_{m=1}^q \left[\theta_{i,2m-1} \sin\left(\frac{2\pi}{w_m}t_j\right) + \theta_{i,2m} \cos\left(\frac{2\pi}{w_m}t_j\right) \right], \quad (24)$$

where $A_{i,m}$ and $\psi_{i,m}$ denote the amplitude and phase of the oscillation with period length w_m . We need to identify $A_{i,m}$ and $\psi_{i,m}$. If we write out

$$\cos\left(\frac{2\pi}{w_m}t_j - \psi_{i,m}\right) = \sin\left(\frac{2\pi}{w_m}t_j\right) \sin \psi_{i,m} + \cos\left(\frac{2\pi}{w_m}t_j\right) \cos \psi_{i,m}$$

we see that we must have

$$A_{i,m} \sin \psi_{i,m} = \theta_{i,2m-1} \quad \text{and} \quad A_{i,m} \cos \psi_{i,m} = \theta_{i,2m}$$

Therefore, we get

$$A_{i,m} = \sqrt{\theta_{i,2m-1}^2 + \theta_{i,2m}^2}, \quad \text{and} \quad (25)$$

$$\psi_{i,m} = \tan^{-1} \left(\frac{\theta_{i,2m-1}}{\theta_{i,2m}} \right). \quad (26)$$

The sets of period, amplitude, and phase $\{w_m, A_{i,m}, \psi_{i,m}\}$, $m = 1, \dots, q$, provide a complete description of the true process $f_i(t_j)$ underlying the observed oscillation.

4 Posterior update

Given the observed data $\mathbf{Y} = \{\mathbf{y}_i\}_{i=1}^p$, we wish to infer the periodic basis functions coefficients $\{\boldsymbol{\theta}_i\}_{i=1}^p$, the local basis functions coefficients $\{\boldsymbol{\gamma}_i\}_{i=1}^p$, the factor loading matrix $\boldsymbol{\Lambda}$, the $T \times k$ matrix of latent factors $\boldsymbol{\eta}$, and all hyperparameters. We use Gibbs sampling by successively drawing samples from the full conditional distributions of each parameter in turn, given all other parameters.

The conditional distribution of \mathbf{Y} implied by (5) is

$$\mathbf{Y}|\mathbf{B}, \mathbf{C}, \boldsymbol{\Theta}, \boldsymbol{\Gamma}, \boldsymbol{\eta}, \boldsymbol{\Lambda}, \boldsymbol{\Sigma} = \prod_{i=1}^p N(\mathbf{y}_i | \mathbf{B}\boldsymbol{\theta}_i + \mathbf{C}\boldsymbol{\gamma}_i + \boldsymbol{\eta}\boldsymbol{\lambda}_i, \sigma_i^2 \mathbf{I}_T), \quad (27)$$

and the likelihood function is

$$\begin{aligned} P(\mathbf{Y}, \boldsymbol{\Theta}, \boldsymbol{\Gamma}, \tilde{\boldsymbol{\Theta}}, \tilde{\boldsymbol{\Gamma}}, \boldsymbol{\Sigma}, \boldsymbol{\eta}, \boldsymbol{\Lambda}, \boldsymbol{\phi}, \boldsymbol{\tau}, \boldsymbol{\varpi}, \boldsymbol{\varpi}^*) = & \quad (28) \\ \prod_{i=1}^p \left\{ N(\mathbf{y}_i | \mathbf{B}\boldsymbol{\theta}_i + \mathbf{C}\boldsymbol{\gamma}_i + \boldsymbol{\eta}\boldsymbol{\lambda}_i, \sigma_i^2 \mathbf{I}_T) \text{Ga}(\sigma_i^{-2} | a_\sigma, b_\sigma) \times \right. \\ N_k \left[\boldsymbol{\lambda}_i^\top | \mathbf{0}, \mathbf{D}_i(\boldsymbol{\phi}, \boldsymbol{\tau}) \right] p(\boldsymbol{\phi} | \rho) p(\boldsymbol{\tau} | a_1, a_2) \prod_{j=1}^T N_k(\boldsymbol{\eta}_j | \mathbf{0}, \mathbf{I}_k) \times \\ N_{2q}(\tilde{\boldsymbol{\theta}}_i | \mathbf{W}\boldsymbol{\lambda}_i, \text{Var}(\boldsymbol{\alpha}_i^\theta)) \times N_{\tilde{T}}(\tilde{\boldsymbol{\gamma}}_i | \mathbf{Z}\boldsymbol{\lambda}_i, \text{Var}(\boldsymbol{\alpha}_i^\gamma)) \times p(K_\theta) \times p(K_\gamma) \times \\ \left. \prod_{j=1}^{2q} N_k(\mathbf{W}_j | \mathbf{0}, \mathbf{I}_k) \times \prod_{j=1}^{\tilde{T}} N_k(\mathbf{Z}_j | \mathbf{0}, \mathbf{I}_k) \times p(\boldsymbol{\varpi}) \times p(\boldsymbol{\varpi}^*) \right\}, \end{aligned}$$

where $p(\boldsymbol{\phi} | \rho)$ and $p(\boldsymbol{\tau} | a_1, a_2)$ are the densities of prior distributions induced by MGSP on vectors of all $\{\phi_{ih}\}_{i=1, \dots, p; h=1, \dots, k}$ and all $\{\tau_h\}_{h=1, \dots, k}$, respectively, and $p(\boldsymbol{\varpi})$ and $p(\boldsymbol{\varpi}^*)$ are the densities of prior distributions induced on vectors of all $\{\varpi_{i,m}\}_{i=1, \dots, p; m=1, \dots, q}$ and $\{\varpi_{i,l}^*\}_{i=1, \dots, p; l=1, \dots, \tilde{T}}$, respectively.

In what follows we use “–” to denote the “rest” of the model, i.e. all random variables not explicitly mentioned in the current state of the Markov Chain. Using the introduced notations we describe a MCMC algorithm for simulation of the full joint posterior distribution of the model parameters.

- *Update of \mathbf{W}* : We place a conjugate normal prior on the columns of the $k \times 2q$ matrix \mathbf{W}^\top , so $\mathbf{W}_l \sim N_k(\mathbf{0}, \mathbf{I}), l = 1, \dots, 2q$. This is equivalent to a prior on the rows of matrix \mathbf{W} , \mathbf{W}_l^\top . Conditioning on the current estimate of $\tilde{\theta}_{i,l} \sim N(\boldsymbol{\lambda}_i^\top \mathbf{W}_l, 1)$ and other model parameters, the posterior update of \mathbf{W}_l is

$$\mathbf{W}_l | - \sim N_k \left(\left(\sum_{i=1}^p \boldsymbol{\lambda}_i \boldsymbol{\lambda}_i^\top + \mathbf{I} \right)^{-1} \left(\sum_{i=1}^p \tilde{\theta}_{i,l} \boldsymbol{\lambda}_i \right), \left(\sum_{i=1}^p \boldsymbol{\lambda}_i \boldsymbol{\lambda}_i^\top + \mathbf{I} \right)^{-1} \right)$$

- *Update of \mathbf{Z}* : We place a conjugate normal prior on the columns of the $k \times \tilde{T}$ matrix \mathbf{Z}^\top , so $\mathbf{Z}_l \sim N_k(\mathbf{0}, \mathbf{I}), l = 1, \dots, \tilde{T}$. This is equivalent to a prior on the rows of matrix \mathbf{Z} , \mathbf{Z}_l^\top . Conditioning on the current estimate of $\tilde{\gamma}_{i,l} \sim N(\boldsymbol{\lambda}_i^\top \mathbf{Z}_l, 1)$ and other model parameters, the posterior update of \mathbf{Z}_l is

$$\mathbf{Z}_l | - \sim N_k \left(\left(\sum_{i=1}^p \boldsymbol{\lambda}_i \boldsymbol{\lambda}_i^\top + \mathbf{I} \right)^{-1} \left(\sum_{i=1}^p \tilde{\gamma}_{i,l} \boldsymbol{\lambda}_i \right), \left(\sum_{i=1}^p \boldsymbol{\lambda}_i \boldsymbol{\lambda}_i^\top + \mathbf{I} \right)^{-1} \right)$$

- *Update of $\boldsymbol{\lambda}_i^\top$* : We place a MGSP on row i of $\boldsymbol{\Lambda}$ (equivalently, column i of $\boldsymbol{\Lambda}^\top$) as in (11). The likelihood contribution factorizes as

$$\begin{aligned} L(\boldsymbol{\lambda}_i | \tilde{\boldsymbol{\Theta}}, \boldsymbol{\Theta}, \tilde{\boldsymbol{\Gamma}}, \boldsymbol{\Gamma}, \boldsymbol{\eta}, \boldsymbol{\Sigma}, \mathbf{W}, \mathbf{Z}) &\propto N_T(\mathbf{y}_i | \mathbf{B}\boldsymbol{\theta}_i + \mathbf{C}\boldsymbol{\gamma}_i + \boldsymbol{\eta}\boldsymbol{\lambda}_i, \sigma_i^2 \mathbf{I}) \times \\ &\times N(\tilde{\boldsymbol{\theta}}_i | \mathbf{W}\boldsymbol{\lambda}_i, \text{Var}(\boldsymbol{\alpha}_i^\theta)) \times N(\tilde{\boldsymbol{\gamma}}_i | \mathbf{Z}\boldsymbol{\lambda}_i, \text{Var}(\boldsymbol{\alpha}_i^\gamma)) \end{aligned} \quad (29)$$

We assume $\text{Var}(\boldsymbol{\alpha}_i^\theta) = \mathbf{I}_{2q}$ and $\text{Var}(\boldsymbol{\alpha}_i^\gamma) = \mathbf{I}_{\tilde{T}}$. The posterior update of $\boldsymbol{\lambda}_i$ is

$$\begin{aligned} \boldsymbol{\lambda}_i | - &\sim N_k \left(\mathbf{V}_{\boldsymbol{\lambda}_i} \mathbf{M}_{\boldsymbol{\lambda}_i}, \mathbf{V}_{\boldsymbol{\lambda}_i} \right), \quad i = 1, \dots, p, \quad \text{where} \\ \mathbf{M}_{\boldsymbol{\lambda}_i} &= \sigma_i^{-2} \boldsymbol{\eta}^\top (\mathbf{y}_i - \mathbf{B}\boldsymbol{\theta}_i - \mathbf{C}\boldsymbol{\gamma}_i) + \mathbf{W}^\top \tilde{\boldsymbol{\theta}}_i + \mathbf{Z}^\top \tilde{\boldsymbol{\gamma}}_i \\ \mathbf{V}_{\boldsymbol{\lambda}_i} &= \left(\frac{1}{\sigma_i^2} \boldsymbol{\eta}^\top \boldsymbol{\eta} + \mathbf{W}^\top \mathbf{W} + \mathbf{Z}^\top \mathbf{Z} + \mathbf{D}_i^{-1} \right)^{-1} \end{aligned} \quad (30)$$

- *Update of $\tilde{\boldsymbol{\theta}}_i$* : We sample the conditional posterior $p(\tilde{\boldsymbol{\theta}}_i | -)$ sequentially for $i = 1, \dots, p$ using a Metropolis-Hastings (MH) sampler conditional on the other model parameters. The MH

proposal originates from a non-thresholded version of the model. Fixing $\mathbb{1}(\|\tilde{\boldsymbol{\theta}}_{i,m}\| \geq \varpi_{i,m}) \equiv 1$ for $m = 1, \dots, q$, we take the proposal distribution to be $N(\tilde{\boldsymbol{\theta}}_i | \mathbf{m}_i, \mathbf{M}_i)$ with

$$\begin{aligned} \mathbf{M}_i &= \left(\sigma_i^{-2} \mathbf{B}^\top \mathbf{B} + \mathbf{I}_{2q} \right)^{-1}, \\ \mathbf{m}_i &= \mathbf{M}_i \times (\sigma_i^{-2} \mathbf{B}^\top \tilde{\mathbf{y}}_i + \mathbf{W} \boldsymbol{\lambda}_i) \end{aligned}$$

with $\tilde{\mathbf{y}}_i = \mathbf{y}_i - \mathbf{C} \boldsymbol{\gamma}_i - \boldsymbol{\eta} \boldsymbol{\lambda}_i$. The candidate is accepted with probability

$$\alpha(\tilde{\boldsymbol{\theta}}_i, \tilde{\boldsymbol{\theta}}_i^*) = \min \left\{ 1, \frac{N(\mathbf{y}_i | \mathbf{B} \boldsymbol{\theta}_i^* + \mathbf{C} \boldsymbol{\gamma}_i + \boldsymbol{\eta} \boldsymbol{\lambda}_i, \sigma_i^2 \mathbf{I}_T) N(\tilde{\boldsymbol{\theta}}_i^* | \mathbf{W} \boldsymbol{\lambda}_i, \mathbf{I}) N(\tilde{\boldsymbol{\theta}}_i | \mathbf{m}_i, \mathbf{M}_i)}{N(\mathbf{y}_i | \mathbf{B} \boldsymbol{\theta}_i + \mathbf{C} \boldsymbol{\gamma}_i + \boldsymbol{\eta} \boldsymbol{\lambda}_i, \sigma_i^2 \mathbf{I}_T) N(\tilde{\boldsymbol{\theta}}_i | \mathbf{W} \boldsymbol{\lambda}_i, \mathbf{I}) N(\tilde{\boldsymbol{\theta}}_i^* | \mathbf{m}_i, \mathbf{M}_i)} \right\}$$

where $\tilde{\boldsymbol{\theta}}_i$ ($\boldsymbol{\theta}_i$) is the current estimate and $\tilde{\boldsymbol{\theta}}_{i,m}^*$ ($\boldsymbol{\theta}_{i,m}^* = \tilde{\boldsymbol{\theta}}_{i,m}^* \mathbb{1}(\|\tilde{\boldsymbol{\theta}}_{i,m}^*\| \geq \varpi_{i,m})$) is the candidate, with $\boldsymbol{\theta}_i^* = \{\boldsymbol{\theta}_{i,m}^*\}_{m=1}^q$.

- *Update of $\tilde{\boldsymbol{\gamma}}_i$:* We sample the conditional posterior $p(\tilde{\boldsymbol{\gamma}}_i | -)$ sequentially for $i = 1, \dots, p$ via MH with proposals obtained from a non-thresholded version of the model. Fixing $\mathbb{1}(\|\tilde{\boldsymbol{\gamma}}_{i,l}\| \geq \varpi_{i,l}^*) \equiv 1$ for $l = 1, \dots, \tilde{T}$, we take the proposal distribution to be $N(\tilde{\boldsymbol{\gamma}}_i | \mathbf{n}_i, \mathbf{N}_i)$ where

$$\begin{aligned} \mathbf{N}_i &= \left(\sigma_i^{-2} \mathbf{C}^\top \mathbf{C} + \mathbf{I}_{\tilde{T}} \right)^{-1}, \\ \mathbf{n}_i &= \mathbf{N}_i \times (\sigma_i^{-2} \mathbf{C}^\top \tilde{\mathbf{y}}_i + \mathbf{Z} \boldsymbol{\lambda}_i) \end{aligned}$$

with $\tilde{\mathbf{y}}_i = \mathbf{y}_i - \mathbf{B} \boldsymbol{\theta}_i - \boldsymbol{\eta} \boldsymbol{\lambda}_i$. The MH acceptance probability is

$$\alpha(\tilde{\boldsymbol{\gamma}}_i, \tilde{\boldsymbol{\gamma}}_i^*) = \min \left\{ 1, \frac{N(\mathbf{y}_i | \mathbf{B} \boldsymbol{\theta}_i + \mathbf{C} \boldsymbol{\gamma}_i^* + \boldsymbol{\eta} \boldsymbol{\lambda}_i, \sigma_i^2 \mathbf{I}_T) N(\tilde{\boldsymbol{\gamma}}_i^* | \mathbf{Z} \boldsymbol{\lambda}_i, \mathbf{I}) N(\tilde{\boldsymbol{\gamma}}_i | \mathbf{n}_i, \mathbf{N}_i)}{N(\mathbf{y}_i | \mathbf{B} \boldsymbol{\theta}_i + \mathbf{C} \boldsymbol{\gamma}_i + \boldsymbol{\eta} \boldsymbol{\lambda}_i, \sigma_i^2 \mathbf{I}_T) N(\tilde{\boldsymbol{\gamma}}_i | \mathbf{Z} \boldsymbol{\lambda}_i, \mathbf{I}) N(\tilde{\boldsymbol{\gamma}}_i^* | \mathbf{n}_i, \mathbf{N}_i)} \right\}$$

where $\tilde{\boldsymbol{\gamma}}_i$ ($\boldsymbol{\gamma}_i$) is the current estimate and $\tilde{\boldsymbol{\gamma}}_{i,l}^*$ ($\boldsymbol{\gamma}_{i,l}^* = \tilde{\boldsymbol{\gamma}}_{i,l}^* \mathbb{1}(\|\tilde{\boldsymbol{\gamma}}_{i,l}^*\| \geq \varpi_{i,l}^*)$) is the candidate, with $\boldsymbol{\gamma}_i^* = \{\boldsymbol{\gamma}_{i,l}^*\}_{l=1}^{\tilde{T}}$.

- *Update of $\varpi_{i,m}$:* The update can be performed via Gibbs sampling conditioning on the current estimate of $\tilde{\boldsymbol{\theta}}_{i,m} = \{\tilde{\theta}_{i,2m-1}, \tilde{\theta}_{i,2m}\}^\top$ and the other model parameters for $i = 1, \dots, p$ and $m = 1, \dots, q$. If $\|\tilde{\boldsymbol{\theta}}_{i,m}\| > K_\theta$ (the upper bound of the uniform prior on $\varpi_{i,m}$), the posterior update of $\varpi_{i,m}$ is

$$\varpi_{i,m} | - \sim \text{Unif}(0, K_\theta).$$

Otherwise, sample

$$\varpi_{i,m} | - \sim \begin{cases} \text{Unif}(0, \|\tilde{\boldsymbol{\theta}}_{i,m}\|) & \text{with probability } \pi^* \\ \text{Unif}(\|\tilde{\boldsymbol{\theta}}_{i,m}\|, K_\theta) & \text{with probability } 1 - \pi^*, \end{cases}$$

with

$$\begin{aligned}\pi^* &= \frac{A}{A + D}, \\ A &= N(\mathbf{y}_i \mid \mathbf{B}_{-m}\boldsymbol{\theta}_{i,-m} + \mathbf{B}_m\tilde{\boldsymbol{\theta}}_{i,m} + \mathbf{C}\boldsymbol{\gamma}_i + \boldsymbol{\eta}\boldsymbol{\lambda}_i, \sigma_i^2 \mathbf{I}_T) \times \|\tilde{\boldsymbol{\theta}}_{i,m}\|, \\ D &= N(\mathbf{y}_i \mid \mathbf{B}_{-m}\boldsymbol{\theta}_{i,-m} + \mathbf{C}\boldsymbol{\gamma}_i + \boldsymbol{\eta}\boldsymbol{\lambda}_i, \sigma_i^2 \mathbf{I}_T) \times (K_\theta - \|\tilde{\boldsymbol{\theta}}_{i,m}\|),\end{aligned}$$

with $N(\mathbf{y}_i \mid \mathbf{m}, \mathbf{v})$ denotes the Gaussian density function with mean \mathbf{m} and covariance matrix \mathbf{v} evaluated at \mathbf{y}_i . Matrix \mathbf{B}_{-m} ($\boldsymbol{\theta}_{i,-m}$) corresponds to the matrix of periodic bases (vector of periodic basis coefficients) with columns (components) $m = \{2m - 1, 2m\}$ excluded. Instead, \mathbf{B}_m ($\tilde{\boldsymbol{\theta}}_{i,m}$) denotes the $\{2m - 1, 2m\}$ -th columns of matrix \mathbf{B} (the $\{2m - 1, 2m\}$ -th components of $\tilde{\boldsymbol{\theta}}_i$).

- *Update of $\varpi_{i,l}^*$* : The update can be performed via Gibbs sampling conditioning on the current estimate of $\tilde{\gamma}_{i,l}$ and the other model parameters for $i = 1, \dots, p$ and $l = 1, \dots, \tilde{T}$. If $|\tilde{\gamma}_{i,l}| > K_\gamma$ (the upper bound of the uniform prior on $\varpi_{i,l}^*$), the posterior update of $\varpi_{i,l}^*$ is

$$\varpi_{i,l}^* \mid - \sim \text{Unif}(0, K_\gamma).$$

Otherwise, sample

$$\varpi_{i,l}^* \mid - \sim \begin{cases} \text{Unif}(0, |\tilde{\gamma}_{i,l}|) & \text{with probability } \pi^* \\ \text{Unif}(|\tilde{\gamma}_{i,l}|, K_\gamma) & \text{with probability } 1 - \pi^*, \end{cases}$$

with

$$\begin{aligned}\pi^* &= \frac{E}{E + F}, \\ E &= N(\mathbf{y}_i \mid \mathbf{B}\boldsymbol{\theta}_i + \mathbf{C}_{-l}\boldsymbol{\gamma}_{i,-l} + \mathbf{C}_l\tilde{\gamma}_{i,l} + \boldsymbol{\eta}\boldsymbol{\lambda}_i, \sigma_i^2 \mathbf{I}_T) \times |\tilde{\gamma}_{i,l}|, \\ F &= N(\mathbf{y}_i \mid \mathbf{B}\boldsymbol{\theta}_i + \mathbf{C}_{-l}\boldsymbol{\gamma}_{i,-l} + \boldsymbol{\eta}\boldsymbol{\lambda}_i, \sigma_i^2 \mathbf{I}_T) \times (K_\gamma - |\tilde{\gamma}_{i,l}|)\end{aligned}$$

Matrix \mathbf{C}_{-l} ($\boldsymbol{\gamma}_{i,-l}$) corresponds to the matrix of local bases (vector of local basis coefficients) with column (component) l excluded. Instead, \mathbf{C}_l ($\tilde{\gamma}_{i,l}$) denotes the l -th column of matrix \mathbf{C} (the l -th component of $\tilde{\boldsymbol{\gamma}}_i$).

Further,

$$\begin{aligned}
K_\theta | - &\sim \text{Pareto} \left(a_\theta + pq, \max\{b_\theta, \max_{i,m} \{\varpi_{i,m}\}_{i=1,m=1}^{p,q}\} \right); \\
K_\gamma | - &\sim \text{Pareto} \left(a_\gamma + p\tilde{T}, \max\{b_\gamma, \max_{i,l} \{\varpi_{i,l}^*\}_{i=1,l=1}^{p,\tilde{T}}\} \right); \\
\sigma_i^{-2} | - &\sim \text{Ga} \left(a_\sigma + \frac{T}{2}, b_\sigma + \frac{\|\mathbf{y}_i - \mathbf{B}\boldsymbol{\theta}_i - \mathbf{C}\boldsymbol{\gamma}_i - \boldsymbol{\eta}\boldsymbol{\lambda}_i\|^2}{2} \right), \quad i = 1, \dots, p; \\
\boldsymbol{\eta}_j | - &\sim N_k \left[\mathbf{V}\boldsymbol{\eta}_j, \mathbf{M}\boldsymbol{\eta}_j, \mathbf{V}\boldsymbol{\eta}_j \right], \quad j = 1, \dots, T, \quad \text{where} \\
&\quad \mathbf{M}\boldsymbol{\eta}_j = \boldsymbol{\Lambda}^\top \boldsymbol{\Sigma}^{-1} (\mathbf{y}^{(j)} - \boldsymbol{\Theta}\mathbf{b}_j - \boldsymbol{\Gamma}\mathbf{c}_j), \\
&\quad \mathbf{V}\boldsymbol{\eta}_j = (\mathbf{I}_k + \boldsymbol{\Lambda}^\top \boldsymbol{\Sigma}^{-1} \boldsymbol{\Lambda})^{-1}; \\
\phi_{ih} | - &\sim \text{Ga} \left(\frac{\rho+1}{2}, \frac{\rho + \tau_h \lambda_{ih}^2}{2} \right), \quad i = 1, \dots, p \quad \text{and} \quad h = 1, \dots, k; \\
\zeta_1 | - &\sim \text{Ga} \left(a_1 + \frac{pk}{2}, 1 + \frac{1}{2} \sum_{l=h}^k \tau_l^{(1)} \sum_{i=1}^p \phi_{il} \lambda_{il}^2 \right); \\
\zeta_h | - &\sim \text{Ga} \left(a_2 + \frac{p}{2}(k-h+1), 1 + \frac{1}{2} \sum_{l=1}^k \tau_l^{(h)} \sum_{i=1}^p \phi_{il} \lambda_{il}^2 \right), \\
&\quad \text{for } h \geq 2, \quad \text{where } \tau_l^{(h)} = \prod_{t=1, t \neq h}^l \zeta_t \quad \text{for } h = 1, \dots, k.
\end{aligned}$$

5 Simulation studies

5.1 Dependence across measurements

We synthesized data from the model, and then used the above framework to infer the model parameters. We simulated \mathbf{y}_i , $i = 1, \dots, p = 500$, from a $T = 24$ -dimensional normal distribution with mean $\mathbf{B}\boldsymbol{\theta}_i + \mathbf{C}\boldsymbol{\gamma}_i + \boldsymbol{\eta}\boldsymbol{\lambda}_i$ and covariance matrix $\sigma_i^2 \times \mathbf{I}_T$, with $\sigma_i^2 = 0.5 \forall i$. The design matrix \mathbf{B} included the Fourier bases as specified in Section 2 with possible periods $\{4, 6, 8, 12, 24\}$ hours, thus $q = 5$, whereas $\tilde{T} = 10$ Gaussian kernels with common bandwidth $\psi = 25$ were chosen for the matrix of local bases \mathbf{C} . The true number of factors was set equal to $k = 6$, and the number of non-zero elements in each column of $\boldsymbol{\Lambda}$ were chosen linearly between $2 \times (10 \log p)$ and $10 \log p + 1$. In practice, this resulted in a number of non-zero elements between 99 and 124 across the different columns of $\boldsymbol{\Lambda}$. We randomly allocated the location of the zeros in each column and simulated the non-zero elements independently from a normal distribution with mean 0 and variance 9. The latent factors $\boldsymbol{\eta}$ were independently generated by sampling from a standard normal distribution.

The $p \times q$ true latent thresholds for Θ were independently generated from a $\text{Unif}(0, 6)$ whereas the $p \times \tilde{T}$ latent thresholds for Γ were independently generated from a $\text{Unif}(0, 10)$ to induce sparsity on Γ and jitter the curves with only a few, time-localized deviations. The rows of \mathbf{W} (\mathbf{Z}) were independently generated by sampling from a standard normal distribution, and the true values of the latent coefficients $\{\tilde{\theta}_i, \tilde{\gamma}_i\}_{i=1}^p$ were generated by sampling from their prior distribution given the true values of \mathbf{W} , \mathbf{Z} , and Λ .

We run the Gibbs sampler described in Section 4 for 50000 iterations with a burn-in of 20000, and collected every 5th sample to thin the chain. The hyperparameters a_σ and b_σ for σ_i^{-2} were 1 and 0.5, respectively, while $\rho = 3$, $a_1 = 2.1$, $a_2 = 3.1$, $a_\theta = a_\gamma = 1$, $\beta_\theta = 5$, $\beta_\gamma = 10$ and used $k = 5$ as the starting number of factors.

Of the 500 curves, 22.4% exhibit simple periodicity with periods either $\{4, 6, 8, 12, 24\}$ hours and the remaining profiles either load on more than one Fourier basis or are pure noise. Only 25 of the 500 simulated profiles truly exhibit circadian expression. Therefore, the signal-to-noise ratio is quite weak in this dataset. Figure 3 shows the estimated trajectories for the 25 circadian variables: the black line represents the true trajectory, the blue line represents the posterior mean estimate of $\mathbf{B}\theta_i + \mathbf{C}\gamma_i + \eta\lambda_i$, and the red dashed lines are the 95% pointwise credible intervals of the same quantity.

[Figure 3 about here.]

Figure 4 shows a comparison between the true correlation (left panel) and the estimated correlation structure (right panel). To improve visibility, the plot only reports probes that give rise to true pair-wise correlations of or above (below) 0.90 (-0.90). The correlation structure seems overall slightly under-estimated: this is likely the effect of the MGPS prior on Λ , which tends to favor small (in magnitude) loadings, as opposed to the wide-support distribution ($N(0, 9)$) used to generate the true non-zero elements on Λ . By examining the correlation matrix generated by probes with *estimated* pair-wise correlation of or above (below) 0.80 (-0.80), we notice an almost perfect match with their true correlation structure (Figure 5).

[Figure 4 about here.]

[Figure 5 about here.]

When computing model-parameter summaries, one must address the fact that the state (zero or non-zero) of the periodic and local basis coefficients $\{\boldsymbol{\theta}_i, \boldsymbol{\gamma}_i\}$ may change between collection of samples (it should change between collection of samples if there is good mixing). When aggregating collection samples, reporting the posterior mean for these parameters could be misleading in that the non-zero estimates will bias the overall posterior mean, which is therefore unlikely to be exactly zero even when the true value of the parameter is zero. Table 1 reports the proportion of posterior samples for which $\boldsymbol{\theta}_m \equiv \{\theta_{i,2m-1}, \theta_{i,2m}\}, m = 1, \dots, 4$ are estimated being equal to zero while $\boldsymbol{\theta}_5 \equiv \{\theta_{i,9}, \theta_{i,10}\}$ are estimated being different from zero for the 25 circadian variables. We recall that $\boldsymbol{\theta}_5$ denotes the vector of coefficients of the sine/cosine bases with 24 hours period. The table also shows the estimated circadian probability (20) and quantiles of the inferred phase and amplitude of the oscillation with period length of 24 hours, $\psi_{i,5}$ and $A_{i,5}$.

[Table 1 about here.]

To assess the performance of the proposed method, we compared our approach with Fisher’s g -test (Wichert et al. 2004), robust g -test (Ahdesmäki et al. 2005), and JTK cycle (Hughes et al. 2010). These methods test the hypothesis of “absence of periodicity” (H_0) versus “signal is periodic” (H_1) with unspecified period. Therefore, the comparison is made by evaluating the estimated probability that a protein is periodic (21). We also compared our method to its “independent” version that is,

$$\mathbf{y}_i = \mathbf{B}\boldsymbol{\theta}_i + \mathbf{C}\boldsymbol{\gamma}_i + \boldsymbol{\epsilon}_i, \quad \boldsymbol{\epsilon}_i \sim N(\mathbf{0}, \sigma_i^2 \mathbf{I}) \quad (31)$$

Model (31) still accommodates local deviations and can detect periodicity, but does not accommodate dependence across variables by blocking inference on \mathbf{A} which is kept fixed to zero. Therefore, it is the default version of our model in scenarios of independence across variables.

For every method, we ordered the p-values (or the estimated circadian probability for our approach) which show how strong the evidence is against the hypothesis of absence of periodic signal. Based on this ordering, we picked-up the first N_i variables from the ordered lists and compared the proportion the true positives, namely the proportion of periodic variables correctly identified as periodic, and the proportion of true negatives, namely the proportion of non-periodic variables correctly classified as non-periodic. Since predictions were periodic or non-periodic, a well-suited binary classification, we applied receiver operating characteristic (ROC) curves to compare the performances of the four algorithms by varying N_i sequentially from $i = 1$ to $i = p$. The performance

is measured by the area under the ROC curve criterion, with the larger area the better method (Figure 6). It is evident that our approach outperforms methods that do not directly accommodate dependence across variables. The grey ROC curve refers to a second chain for our model initialized at over-dispersed starting values; it is used to check the reproducibility of the results. The right panel of Figure 6 shows the progression of the false discovery rate (FDR) as function of the true positive rate (power). The FDR is defined as the ratio between false positives, namely the number of variables falsely declared as periodic, and the number of positives, namely the total number of variables declared periodic. The spike at 0 for Fisher’s g -test and robust g -test means that the protein with smallest p-value, thus the first selected as periodic, is in fact a false positive. The more variables we include in the list of periodic variables, the more the power increases. A value of power equal to 1 corresponds to detection of all truly periodic variables as periodic. For large values of power, our model achieves lower FDR than methods which do not accommodate dependence.

Several chains were run to assess the sensitivity of the results to different choices of $a_\theta, a_\gamma, b_\theta, b_\gamma$, and other model parameters. In all cases, our approach achieved better performance than methods not accommodating dependence across variables.

[Figure 6 about here.]

5.2 Independence across measurements

For any modeling approach which accommodates dependence across variables, one concern is that if the true profiles are indeed independent, whether the “unnecessarily sophisticated” dependent-modeling approach can perform as good as the “correct, independent” model.

To test the performance of our proposed method in such case, we simulated sample paths from the model but fixed $\mathbf{\Lambda} \equiv \mathbf{0}$ such that at any time point $j = 1, \dots, T$ the variables were independent of each other, $\mathbf{y}^{(j)} \sim N(\mathbf{\Theta}\mathbf{b}_j + \mathbf{\Gamma}\mathbf{c}_j, \mathbf{\Sigma})$, with $\mathbf{\Sigma}$ diagonal. We increased σ_i^2 to 1, $\forall i$ and generated the $p \times q$ true latent thresholds for $\mathbf{\Theta}$ independently from a $\text{Unif}(0, 5)$. All remaining parameters were generated as described in Section 5.1. Of the $p = 500$ simulated trajectories, 4% were circadian and 78 were periodic with possible periods either 4, 6, 8, 12 or 24 hours.

We run the Gibbs sampler described in Section 4 for 50000 iterations with a burn-in of 20000, and collected every 5th sample to thin the chain. The hyperparameters a_σ and b_σ for σ_i^{-2} were 1 and 0.5, respectively, while $\rho = 3$, $a_1 = 2.1$, $a_2 = 3.1$, $a_\theta = a_\gamma = 1$, $\beta_\theta = \beta_\gamma = 5$ and used $k = 4$ as

the starting number of factors.

The additional complexity does not affect our method, which still outperforms Fisher’s g -test, robust g -test and JTK cycle and performs at least as well as its corresponding independent version (Figure 7). The good performance has to be attributed to the shrinkage property of the MGSPSP. Figure 8 shows side-by-side boxplots of the posterior mean estimate of the factor loadings that is, the posterior means of $\{\mathbf{\Lambda}_{1:p,1}, \mathbf{\Lambda}_{1:p,2}, \dots, \mathbf{\Lambda}_{1:p,k=6}\}$, where $k = 6$ is the posterior mean of the estimated number of factors. Although this prior can not return exactly zero estimates for the components of $\mathbf{\Lambda}$, the estimated factor loadings are small in magnitude, thus shrinking toward the truth (zero) the contribution of $\boldsymbol{\eta}\boldsymbol{\lambda}_i$ in (5).

[Figure 7 about here.]

[Figure 8 about here.]

6 Analysis of mouse liver mRNA data

We apply our method to a real dataset generated from the work of Jouffe et al. (2013). The goal of the study was to assess whether the circadian clock could coordinate the transcription of messenger RNA (mRNA) in mouse liver. In the experiment, C57B1/6J male mice between 10 and 12 weeks of age were used. Mice were maintained under standard animal housing conditions, with free access to food and water and in 12 hours light/12 hours dark cycles. However, mice were fed only at night during 4 days before the experiment to reduce the effects of feeding on rhythm. In the case of rodents, it is in fact during the night period that animals are active and consume food. Liver polysomal and total RNAs were extracted independently from two mice sacrificed every 2 hours during 48 hours. 3 μg of polysomal and total RNAs from each animal from each time point were pooled. The 6 μg of polysomal and total mRNAs were used for the synthesis of biotinylated complimentary RNAs (cRNAs) according to Affymetrix protocol, and the fluorescence signal was analyzed with Affimetrix software (refer to Jouffe et al. (2013) for more details on the study). Data are deposited on the Gene Expression Omnibus database under the reference GSE33726. In the original study, the rhythmic characteristics of the expression of each gene or protein were assessed by a Cosinor analysis (Nelson et al. 1979), and a rhythm was detected if the null hypothesis was rejected with p -value < 0.05 . A period of 24 hours was considered a priori. Consequently, the

authors validated as circadian a subset of the detected genes and encoded proteins in laboratory. The authors concluded that the circadian clock influences the temporal translation of a subset of mRNAs mainly involved in ribosome biogenesis. In addition, the circadian clock appeared to regulate the transcription of ribosomal protein mRNAs and ribosomal RNAs.

We considered a randomly selected subset of $p = 1000$ proteins from the full dataset. The raw expression levels were log-transformed and normalized to zero-mean following standard practice. We run the Gibbs sampler described in Section 4 for 50000 iterations with a burn-in of 20000, and collected every 5th sample to thin the chain. The hyperparameters a_σ and b_σ for σ_i^{-2} were 1 and 0.5, respectively, while $\tilde{T} = 20, \rho = 3, a_1 = 2.1, a_2 = 3.1, a_\theta = a_\gamma = 1, \beta_\theta = 6, \beta_\gamma = 10$ and used $k = 8$ as the starting number of factors.

Using our model, we ranked the probes by their posterior probability of being periodic (21), and Figure 9 shows the top 20 probes. Of the top 20 (50) probes, 19 (42) of them also rank among the top 20 (50) by posterior probability of being circadian. We also tested the probes with Fisher’s g -test, JTK cycle, and the independent version of our approach and compared the top 100 probes by evidence against the null hypothesis of absence of periodicity (by p-value or posterior probability of being periodic). Of these top 100 probes, 50 are shared with JTK cycle, 47 with Fisher’s g -test, and 61 with the independent version of our method. All together, the four methods agreed on a common set of 36 probes as most likely to be periodic.

[Figure 9 about here.]

A key attractive feature of our model is the accommodation of dependence across proteins, thus it becomes of interest to examine the inferred correlation structure of the 1000 proteins from the estimated covariance $\mathbf{\Omega} = \mathbf{\Lambda}\mathbf{\Lambda}^\top + \mathbf{\Sigma}$. Most of the estimated correlations are small in magnitude and only 104 pairs of probes have correlation equal or above 0.30 (in absolute value). These “major” correlations are controlled by only 27 (dominant) probes linked (positively or negatively) to each other as shown in Figure 10. By inspecting the plot, one can envision two groups of probes: one group with proteins 1 – 13 in the bottom left corner and the second group with proteins 14 – 27 in the top right corner. Correlation is positive within each group and negative across groups. To be more conservative, we can further restrict to a set of 8 proteins with estimated correlation of or above 0.45 (in absolute value) as shown in Figure 11. Again, these 8 proteins divide into 2 groups: group 1 with probes 1423069 AT, 1424251 A AT, 1424962 AT, 1426644 AT, 1427200 AT;

and group 2 with probes 1419450 AT, 1435068 AT, 1436064 X AT. Proteins within each group are positively correlated with each other, whereas the correlation is negative across groups. Proteins in each group exhibit a common pattern in normalized expression level (Figure 12). Proteins in group 1 exhibit a dip in their normalized expression levels between 10 and 30 hours, as opposed to the peak that probes in group 2 exhibit. Although local deviation seem to emerge in the trajectories of proteins in group 2, the sequence of dips and peaks over time seems overall reversed in the two groups.

[Figure 10 about here.]

[Figure 11 about here.]

[Figure 12 about here.]

7 Conclusions

A flexible Bayesian methodology for periodicity detection has been developed and applied to large-scale circadian gene expression studies. It employs a Fourier basis expansion with variable selection priors on the basis coefficients to model the time course gene expression trajectories and identify rhythmic genes. The key statistical contribution is to accommodate the potential dependence in the trajectories in terms of latent factors. Our construction allows to infer groups of co-expressed collections of genes and verify relationships within and across groups. Further, accommodating dependence helps identifying weaker patterns appearing in expression profiles by sharing information across genes. Simulation studies show that our construction gives significantly improved performance over widely-used rhythmicity detection techniques that do not directly accommodate for dependence across genes.

References

- Ahdesmäki, M., Lähdesmäki, H., Pearson, R., Huttunen, H. & Yli-Harja, O. (2005), ‘Robust detection of periodic time series measured from biological systems’, *BMC Bioinformatics* **6**, 118.
- Anderson, P. E., Smith, J. Q., Edwards, K. D. & Millar, A. J. (2006), Guided conjugate bayesian

clustering for uncovering rhythmically expressed genes, Working paper.

URL: <http://wrap.warwick.ac.uk/35566/>

- Bhattacharya, A. & Dunson, D. B. (2011), ‘Sparse Bayesian infinite factor models’, *Biometrika* **98**(2), 291–306.
- Chudova, D., Ihler, A., Lin, K. K., Andersen, B. & Smyth, P. (2009), ‘Bayesian detection of non-sinusoidal periodic patterns in circadian expression data’, *Bioinformatics* **25**(23), 3114–3120.
- Costa, M. J., Finkenstädt, B., Roche, V., Lévi, F., Gould, P. D., Foreman, J., Halliday, K., Hall, A. & Rand, D. a. (2013), ‘Inference on periodicity of circadian time series’, *Biostatistics* **14**(4), 792–806.
- Dodd, A. N., Gardner, M. J., Hotta, C. T., Hubbard, K. E., Dalchau, N., Love, J., Assie, J.-M., Robertson, F. C., Jakobsen, M. K., Goncalves, J., Sanders, D. & Webb, A. A. R. (2007), ‘The *arabidopsis* circadian clock incorporates a cadpr-based feedback loop’, *Science* **318**, 1789–1792.
- Edwards, K. D., Anderson, P. E., Hall, A., Salathia, N. S., Locke, J. C. W., Lynn, J. R., Straume, M., Smith, J. Q. & Millar, A. J. (2006), ‘Flowering locus *c* mediates natural variation in the high-temperature response of the *arabidopsis* circadian clock’, *The Plant Cell* **18**, 639–650.
- Heard, N. A., Holmes, C. C. & Stephens, D. A. (2006), ‘A quantitative study of gene regulation involved in the immune response of anopheline mosquitoes: an application of bayesian hierarchical clustering of curves’, *Journal of the American Statistical Association* **101**, 18–29.
- Hughes, M. E., Hogenesch, J. B. & Kornacker, K. (2010), ‘JTK_CYCLE: an efficient nonparametric algorithm for detecting rhythmic components in genome-scale data sets’, *Journal of Biological Rhythms* **25**(5), 372–380.
- Jouffe, C., Cretenet, G., Symu, L., Martin, E., Atger, F., Naef, F. & Gachon, F. (2013), ‘The circadian clock coordinates ribosome biogenesis’, *PLoS Science* **11**.
- Liverani, S. (2009), Bayesian clustering of curves and the search of the partition space, PhD thesis, University of Warwick, UK.
- Luan, Y. & Li, H. (2003), ‘Clustering of time-course gene expression data using a mixed-effects model with b-splines’, *Bioinformatics* **19**, 474–482.

- Müller, P., Parmigiani, G. & Rice, K. (2006), ‘Fdr and bayesian multiple comparisons rules’, *Johns Hopkins University, Dept. of Biostatistics Working Papers* .
- Müller, P., Parmigiani, G., Robert, C. & Rousseau, J. (2004), ‘Optimal sample size for multiple testing: the case of gene expression microarrays’, *Journal of the American Statistical Association* **99**, 990–1001.
- Nakajima, J. & West, M. (2013), ‘Bayesian analysis of latent threshold dynamic models’, *Journal of Business and Economic Statistics* **31**, 151–164.
- Nelson, W., Tong, Y. L., Lee, J. K. & F., H. (1979), ‘Methods for cosinor-rhythmometry’, *Chronobiologia* **6**, 305–323.
- Newton, M. A., Noueiry, A., Sarkar, D. & Ahlquist, P. (2004), ‘Detecting differential gene expression with a semiparametric hierarchical mixture method’, *Biostatistics* **5**(2), 155–176.
- Straif, K., Baan, R., Grosse, Y., Secretan, B., El Ghissassi, F., Bouvard, V., Altieri, A., Benbrahim-Tallaa, L. & Coglianò, V. (2007), ‘Carcinogenicity of shift-work, painting, and fire-fighting’, *The Lancet Oncology* **8**(12), 1065–1066.
- Straume, M. (2004), ‘Dna microarray time series analysis: automated statistical assessment of circadian rhythms in gene expression patterning’, *Methods in enzymology* **383**, 149–166.
- Wakefield, J., Zhou, C. & Self, S. (2003), Modeling gene expression over time: curve clustering with informative prior distributions, in J. M. Bernardo, M. Bayarri, J. Berger, A. Dawid, D. Heckerman, A. F. M. Smith & M. West, eds, ‘Bayesian Statistics 7’, Oxford University Press.
- Wichert, S., Fokianos, K. & Strimmer, K. (2004), ‘Identifying periodically expressed transcripts in microarray time series data’, *Bioinformatics* **20**(1), 5–20.
- Yeung, K. Y., Fraley, C., Murua, A., Raftery, A. E. & Ruzzo, W. L. (2001), ‘Model-based clustering and data transformations for gene expression data’, *Bioinformatics* **17**, 977–987.

A Appendix: Analysis of *Arabidopsis* circadian expression data

We apply our method to a real dataset generated from the work of Edwards et al. (2006) in the study of the *Arabidopsis* circadian system. The study was designed to detect genes whose expression levels may be connected with the circadian clock. Eight-day-old Columbia seedlings grown under 12-hours-light / 12-hours-dark cycles were transferred to constant light at 22°. Plant samples were harvested at 13 time points, covering two circadian cycles in 4 hours intervals, starting 26 hours after the last dark-light transition. RNA prepared from these samples was analyzed using Affymetrix ATH1 microarrays. In the original study of Edwards et al. (2006), the authors used COSOPT (Straume 2004) to identify cyclic genes. Of 22810 genes, 3504 genes were considered rhythmic at a significance threshold of $\text{pMMC-}\beta < 0.05$ ($\text{pMMC-}\beta$ measures the probability for multiple testing, similarly to the FDR q -value).

The raw expression levels were standardized following standard practice. We run the Gibbs sampler described in Section 4 for 40000 iterations with a burn-in of 20000, and collected every 10th sample to thin the chain. The hyperparameters a_σ and b_σ for σ_i^{-2} were 1 and 0.5, respectively, while $\rho = 3$, $a_1 = 2.1$, $a_2 = 3.1$, $a_\theta = a_\gamma = 1$, $\beta_\theta = 6$, $\beta_\gamma = 8$ and used $k = 8$ as the starting number of factors. Ten B-splines bases ($\tilde{T} = 10$) were chosen for the matrix of local basis functions.

Our dependent latent factor approach assigned an estimated circadian probability of or above 0.80 to 1419 genes, thus was more conservative than COSOPT. Of these genes, 1319 were shared with COSOPT. If we want to be less conservative and define circadian all those genes with estimated posterior circadian probability of or above 0.70, 0.60 or 0.50, respectively, then the number of detected genes increases to 1933, 2416, and 2845, respectively. Figure 14 shows 6 well-known clock genes by biological knowledge of the *Arabidopsis* dataset that also rank top by posterior probability of being circadian. An inspection of the top circadian genes confirmed sinusoidal patterns through time with a period of approximately 24 hours.

[Figure 13 about here.]

Unfortunately, there is no way to compare the potentially incoherent findings of different statistical approaches on a real dataset in that there is no such a thing as the truth in absence of exact biological validation that supports or contradicts any conclusion. However, a more recent study (Dodd et al. 2007) reported 26 well-known clock-associated genes in *Arabidopsis*. Among these genes

are CCA1 (Circadian Clock Associated 1) and LHY (Late Elongated Hypocotyl), which function synergistically in regulating circadian rhythms of *Arabidopsis*, TOC1 (Timing of Cab Expression 1), which contributes to the plant fitness (carbon fixation, biomass) by influencing the circadian clock period, and ELF4 (Early Flowering 4), which accounts for sustained rhythms in the absence of daily light/dark cycles. ELF4 is necessary for light-induced expression of both CCA1 and LHY, and conversely, CCA1 and LHY act negatively on light-induced ELF4 expression. We used these genes as benchmark to evaluate our approach in terms of false negatives for analyzing circadian expression data. For computational convenience, we only examined a subset of 5000 genes which included the 26 known-clock genes and ranked the probes in order of significance against the null hypothesis of absence of periodicity. The rankings of the 26 known clock genes for the different algorithm is reported in Table 2. All the algorithms were able to identify most of the known clock genes from among their top 25% ranked candidates. The complete list of estimated posterior circadian probability for these 26 known clock genes is reported in Table 3. Interestingly, the genes with lowest circadian probability (below 0.10) also rank as least likely to be circadian among the 26 known clock-genes with other approaches.

It is interesting to examine the inferred correlation structure among the 26 known clock genes. Figure 11 shows the inferred network among these 26 genes by thresholding their estimated correlation with lines connecting genes whose pairwise estimated correlation is above 0.05. If genes are not connected then the corresponding pairwise correlation with other genes falls below this threshold. Essentially, two groups are learnt and the examination of their raws curves seems to confirm trajectories of opposite phases.

[Table 2 about here.]

[Table 3 about here.]

[Figure 14 about here.]

Table 1: Simulation study as of Section 5.1: columns refer to the different periodic basis parameters and rows to the truly circadian variables. Columns 2-5 report the proportion of posterior samples for which $\boldsymbol{\theta}_m = \{\theta_{i,2m-1}, \theta_{i,2m}\}$ are estimated being equal to zero for $m = 1, \dots, 4$, whereas column 6 reports the proportion of posterior samples for which $\boldsymbol{\theta}_5 = \{\theta_{i,9}, \theta_{i,10}\}$ are estimated being different from zero. Vector $\boldsymbol{\theta}_5$ contains the coefficients of the oscillation with period length of 24 hours. Column 7 reports the estimated probability of a protein being circadian, i.e. the proportion of posterior samples with $\{\theta_{i,m}\}_{m=1}^{2q-2} \equiv 0$ and $\{\theta_{i,2q-1}, \theta_{i,2q}\} \neq \mathbf{0}$. The last two columns report the true amplitude and phase versus the [2.5, 50, 97.5]% quantiles of estimated amplitude and phase for the oscillation with period length of 24 hours (brackets). Ranking is by posterior circadian probability.

Protein	$\boldsymbol{\theta}_{i,1}$	$\boldsymbol{\theta}_{i,2}$	$\boldsymbol{\theta}_{i,3}$	$\boldsymbol{\theta}_{i,4}$	$\boldsymbol{\theta}_{i,5}$	P(Circ)	$A_{i,5}$ (true/est)	$\psi_{i,5}$ (true/est)
66	100	100	100	100	100	1	4.84 [4.1, 4.5, 4.9]	0.48 [0.47, 0.50, 0.52]
251	100	99.7	95.1	99.9	100	0.95	1.46 [1.4, 1.4, 1.4]	1.53 [-1.28, -1.28, -1.28]
489	98.5	98.7	99.3	97.5	100	0.94	4.09 [3.22, 3.73, 4.46]	0.35 [0.25, 0.38, 0.45]
387	96	97.3	100	100	99.9	0.93	0.75 [0.86, 0.86, 0.98]	0.14 [-0.67, -0.67, -0.56]
41	91.4	99	99.6	97.6	100	0.88	1.26 [1.09, 1.37, 1.66]	0.54 [0.34, 0.49, 0.76]
417	87.4	99	100	100	100	0.87	1.44 [1.23, 1.23, 1.23]	1.23 [1.1, 1.1, 1.1]
382	95.8	93.6	94.1	94.4	100	0.80	1.38 [1.68, 2.29, 2.78]	0.87 [0.58, 0.86, 1.1]
477	92.8	94.1	94.2	87.7	100	0.72	4.09 [2.19, 3.14, 4.26]	0.33 [0.01, 0.41, 0.65]
255	75.8	92.6	98.8	98.9	100	0.69	2.43 [1.73, 1.89, 2.4]	0.26 [0.18, 0.44, 0.6]
160	66.5	95.7	99.1	93.4	100	0.59	1.85 [1.43, 1.7, 2.13]	1.07 [0.65, 0.9, 1.12]
70	94.9	98.1	99	98.3	81.4	0.57	0.92 [0.45, 0.7, 1.12]	-0.39 [-1.32, -0.83, 1.51]
435	97.5	99.4	62.4	96.3	99.8	0.57	1.48 [0.71, 0.73, 1.35]	0.47 [-0.01, 0.35, 0.69]
87	92.2	75.6	83.4	97.5	93.9	0.53	1.66 [0.77, 1.28, 1.94]	1.3 [-1.56, -1.04, 1.54]
37	87.9	85	79	88.9	98.8	0.53	4.96 [1.44, 2.78, 4.11]	-0.33 [-0.67, -0.17, 0.32]
430	93.4	99	56.5	98.1	100	0.52	1.84 [1.91, 2.09, 2.3]	1.09 [0.98, 1.16, 1.27]
353	88	72.6	88.8	90.8	98.8	0.51	4.11 [1.71, 2.76, 4.02]	-0.08 [-0.42, 0.11, 0.56]
80	82.3	81.9	81.6	72.5	87.6	0.35	5.73 [1.11, 2.75, 4.42]	0.15 [-0.42, 0.48, 1.21]
461	99.6	33.4	99.1	98.4	100	0.32	3.8 [2.86, 4.16, 4.16]	0.21 [-0.08, 0.03, 0.17]
379	93.8	99	98.4	91.9	36.8	0.28	0.56 [0.55, 1.03, 1.3]	-0.75 [-1.42, -1.4, -0.36]
400	79.7	74.4	82.6	82.3	64.4	0.26	4.06 [0.78, 2.21, 4.54]	-1.41 [-1.54, 0.94, 1.54]
356	93.8	95.7	93.4	26.1	100	0.20	3.79 [2.26, 3.45, 4.03]	-0.05 [-0.37, 0.04, 0.17]
176	95.3	98.7	98.2	6.7	100	0.06	1.18 [0.67, 0.92, 1.35]	0.67 [0.14, 0.56, 1.02]
105	75.8	19	96.5	37.7	99.7	0.06	2.56 [1.15, 1.71, 3.62]	-0.08 [0.12, 0.7, 0.97]
67	92.1	5.5	99.9	67.7	100	0.04	1.27 [0.85, 1.2, 1.64]	-1.31 [-1.5, -1.17, -0.86]
373	86.8	96.6	98.2	69.7	3	0.02	0.49 [0.29, 0.56, 1.17]	-0.28 [-0.9, 0.12, 1.37]

Table 2: Summary of rankings of 26 known clock genes from a subset of 5,000 probes in the *Arabidopsis* genome. The ranking of genes was done by posterior circadian probability for our dependent latent factor approach and its independent version (IndepV); by p -value for JTK cycle; by FDR q -value for Fisher’s g -test.

Method	Top 1%	Top 5%	Top 10%	Top 25%	Top 60%
Dep. LF	4	11	17	23	25
IndepV	2	6	13	22	25
Fisher’s g	2	9	14	20	25
JTK cycle	1	8	12	17	22

Table 3: Posterior estimate of circadian probability for the 26 known clock genes in a subset of 5000 probes randomly chosen from the entire genome of *Arabidopsis*. Clock genes are identified by their AGI code and Alias name.

AGI	Alias	P(circadian)	AGI	Alias	P(circadian)
At5g15850	COL1	0.99	At2g46340	SPA1	0.33
At3g02380	COL2	0.99	At2g21660	GRP7	0.32
At2g40080	ELF4	0.99	At2g25930	ELF3	0.30
At1g01060	LYH	0.99	At5g24470	PRR5	0.30
At1g04400	CRY2	0.98	At1g22770	GI	0.12
At5g02810	PRR7	0.97	At4g08920	CRY1	0.08
At5g61380	TOC1	0.94	At4g39260	GRP8	0.02
At3g46640	LUX	0.91	At2g46790	PRR9	0.02
At5g60100	PRR3	0.80	At5g35840	PHYC	0.02
At2g46830	CCA1	0.68	At5g59560	SRR1	0.01
At2g18790	PHYB	0.65	At5g57360	ZTL	0.01
At1g09570	PHYA	0.35	At4g16250	PHYD	0.003
At4g18130	PHYE	0.33	At2g18915	LKP2	5e-04

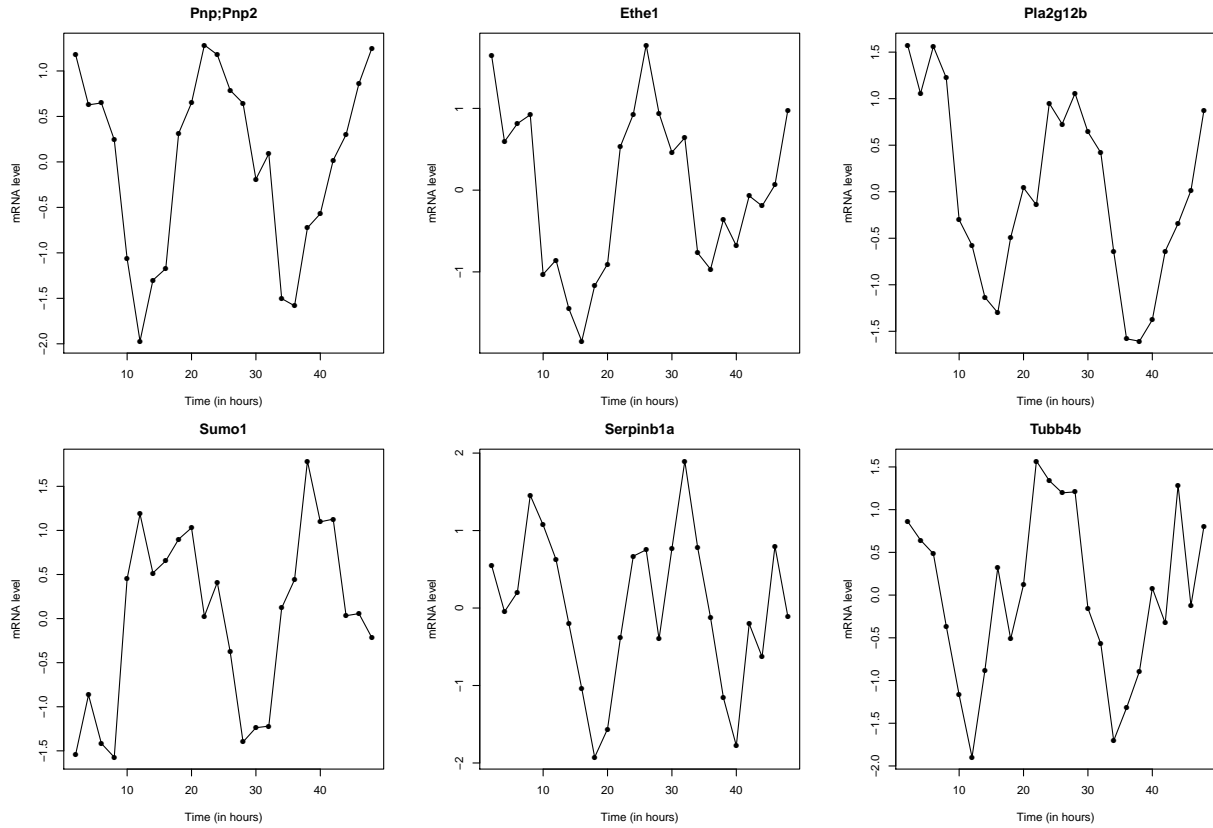


Figure 1: Examples of temporal mRNA expression profiles of rhythmically translated genes as selected by our approach from Jouffe et al. (2013) microarray dataset. Data are log transformed and normalised following standard procedure.

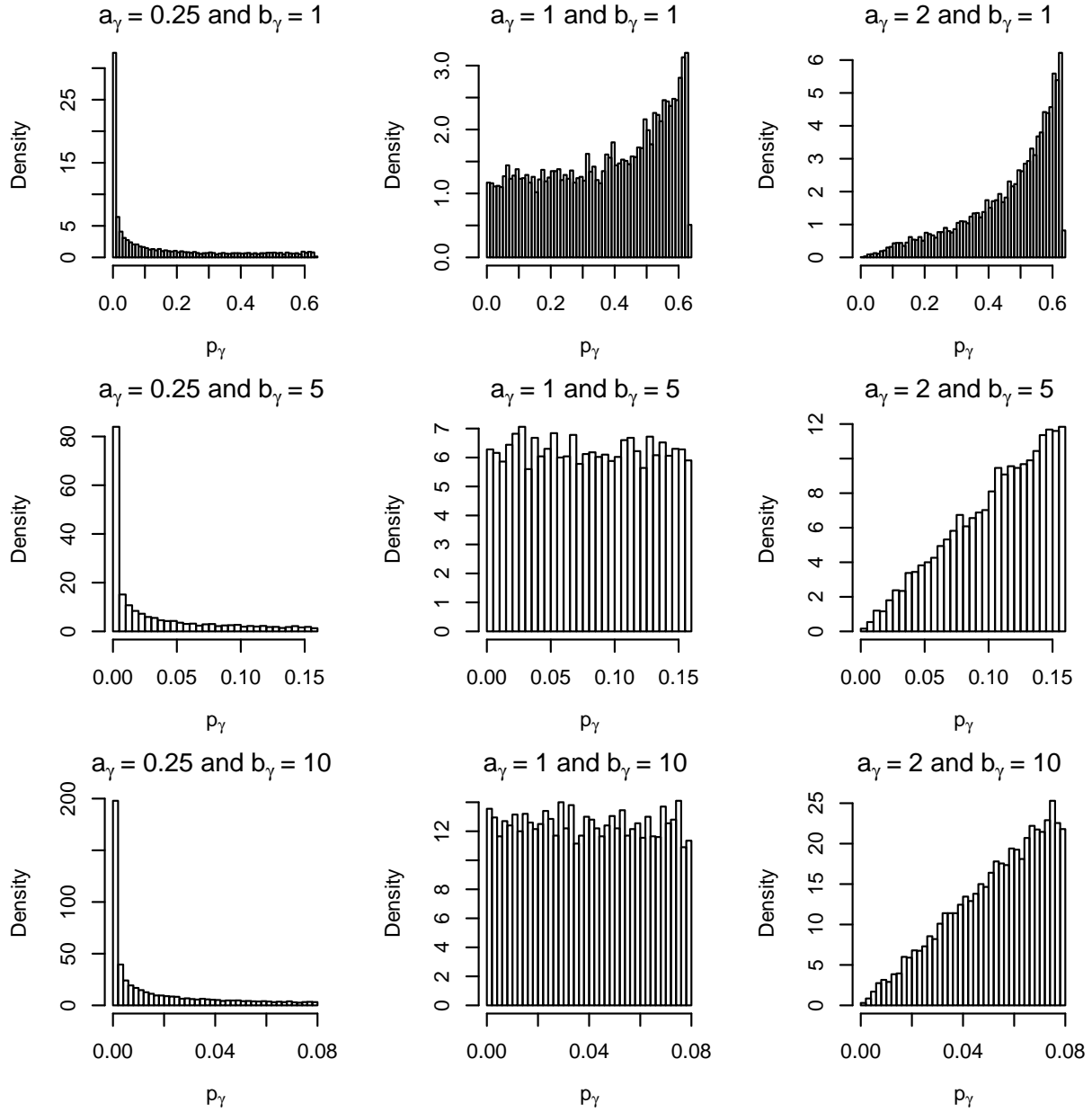


Figure 2: Distribution of the prior probability of non-shrinkage of the local basis coefficients, $p_\gamma := Pr(\gamma_{i,l} \neq 0 \mid K_\gamma)$, for different choices of Pareto hyperparameters a_γ and b_γ .

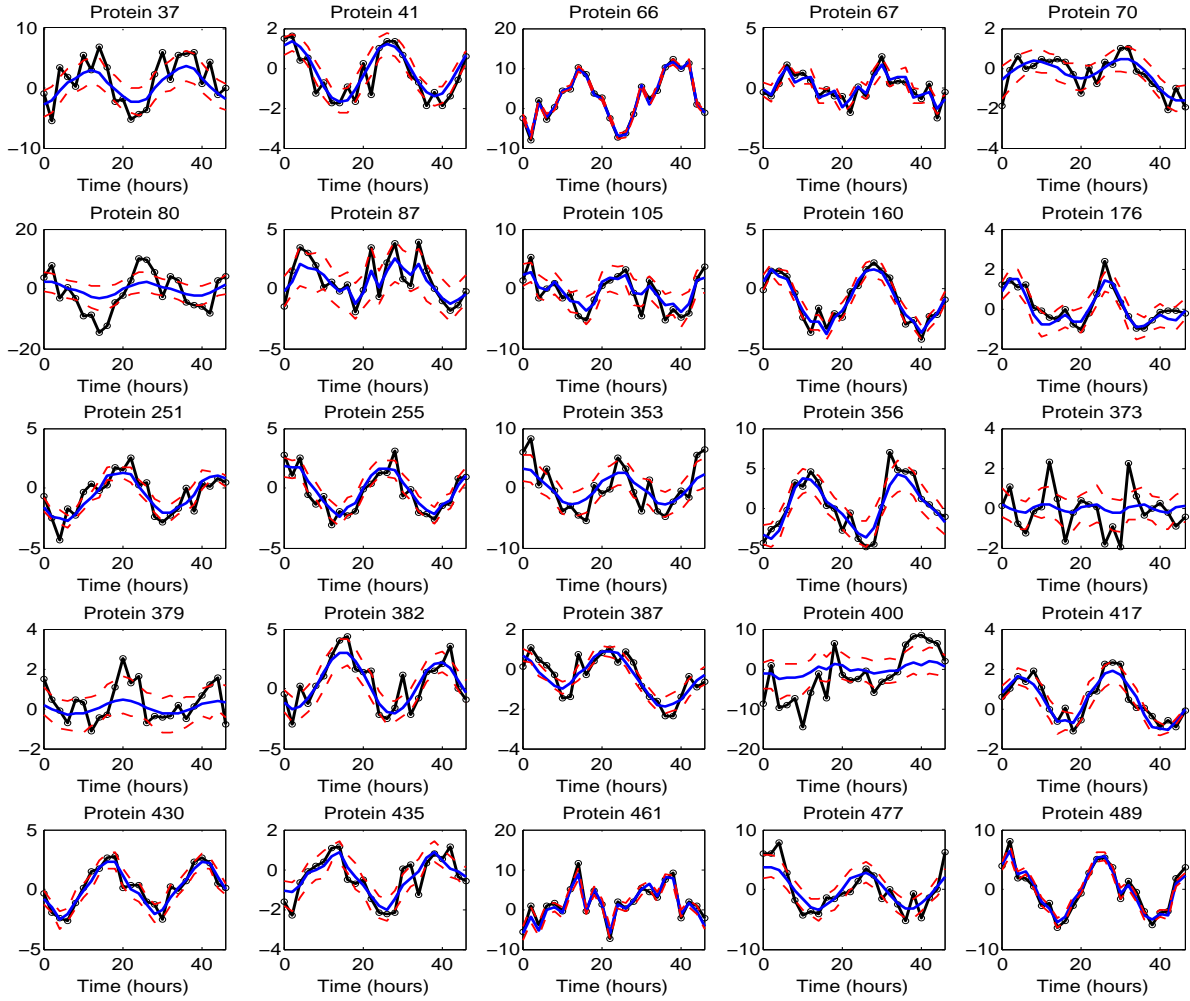


Figure 3: True (black) and inferred (blue) trajectories of the 25 truly circadian variables in the simulation study of Section 5.1, with the horizontal axis corresponding to time. Red lines are the pointwise 95% credible intervals.

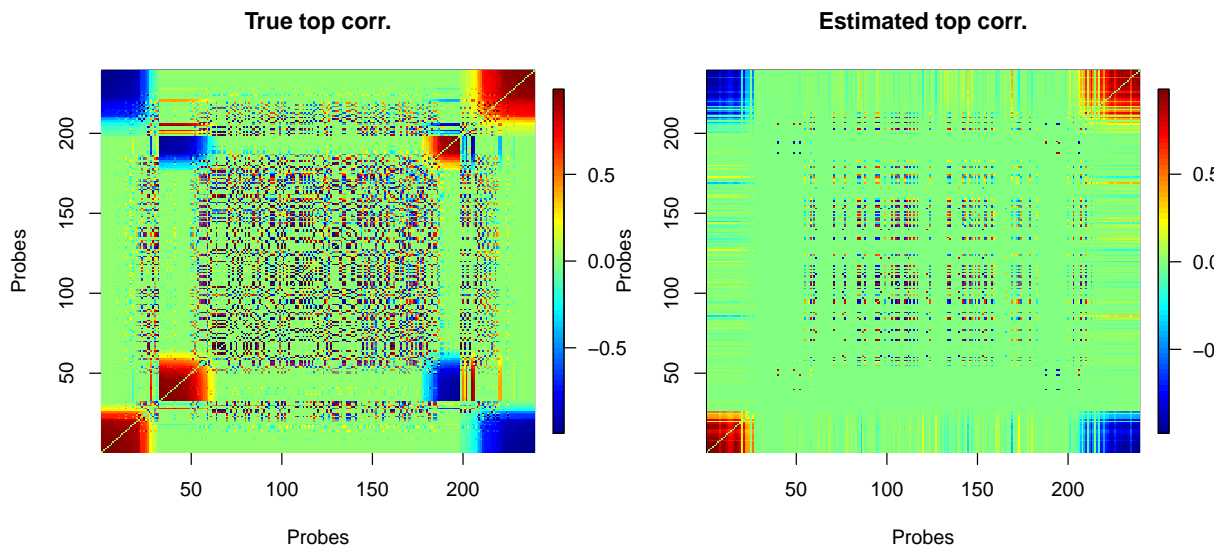


Figure 4: Comparison between true and estimated correlation structure among probes with true pair-wise correlation of or above (below) 0.90 (-0.90). To improve visibility, the diagonal of the correlation matrix is set equal to 0.

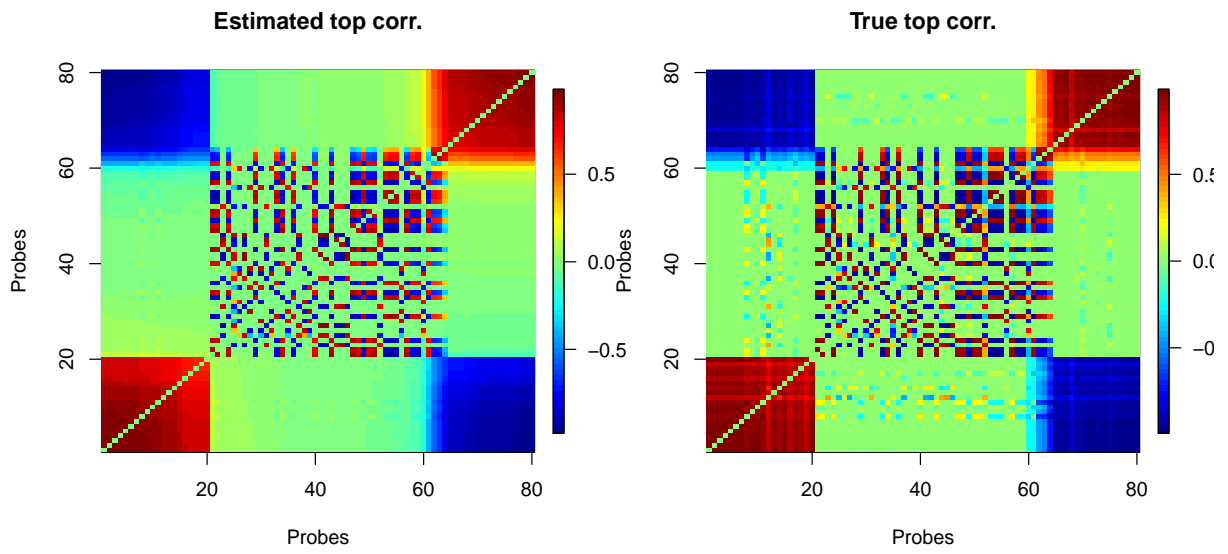


Figure 5: Comparison between estimated and true correlation structure among probes with estimated pair-wise correlation of or above (below) 0.80 (-0.80). To improve visibility, the diagonal of the correlation matrix is set equal to 0.

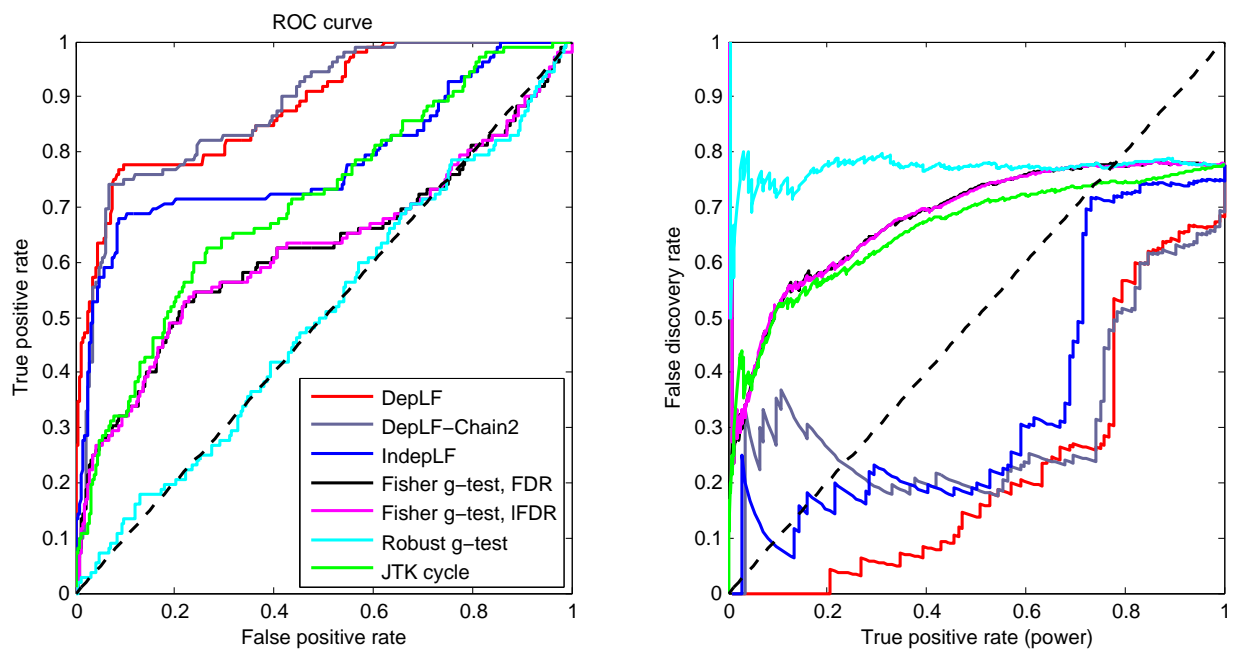


Figure 6: Left panel: ROC curve for identifying periodic signals in the simulated example with dependence across variables. Right panel: progression of false discovery rate (FDR) for different levels of true positive rate. Two chains initialized at over-dispersed starting values were run to assess the reproducibility of the results, and these chains correspond to the red and grey lines. The blue line corresponds to the “independent” version of our method as in (31). Multiple testing for Fisher’s g -test is done using tail area-based FDR and density-based local FDR (lFDR).

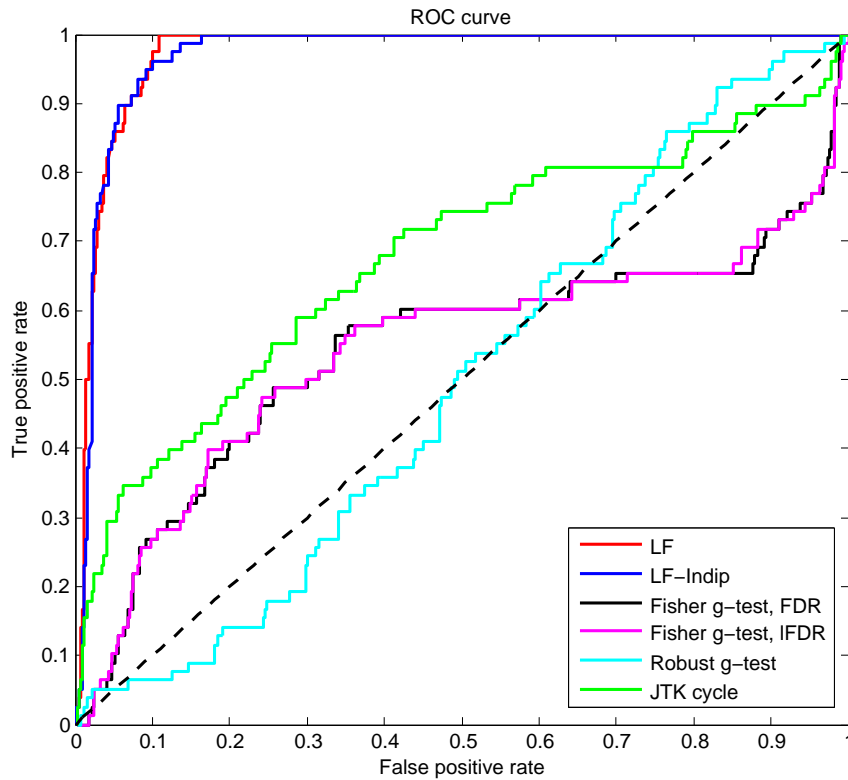


Figure 7: ROC curve for identifying periodic signals in the simulated example with independence across variables. The blue curve refers to the “independent” version of our method obtained by keeping Λ fixed to zero. Multiple testing for Fisher’s g -test is done using tail area-based false discovery rate (FDR) and density-based local false discovery rate (lFDR).

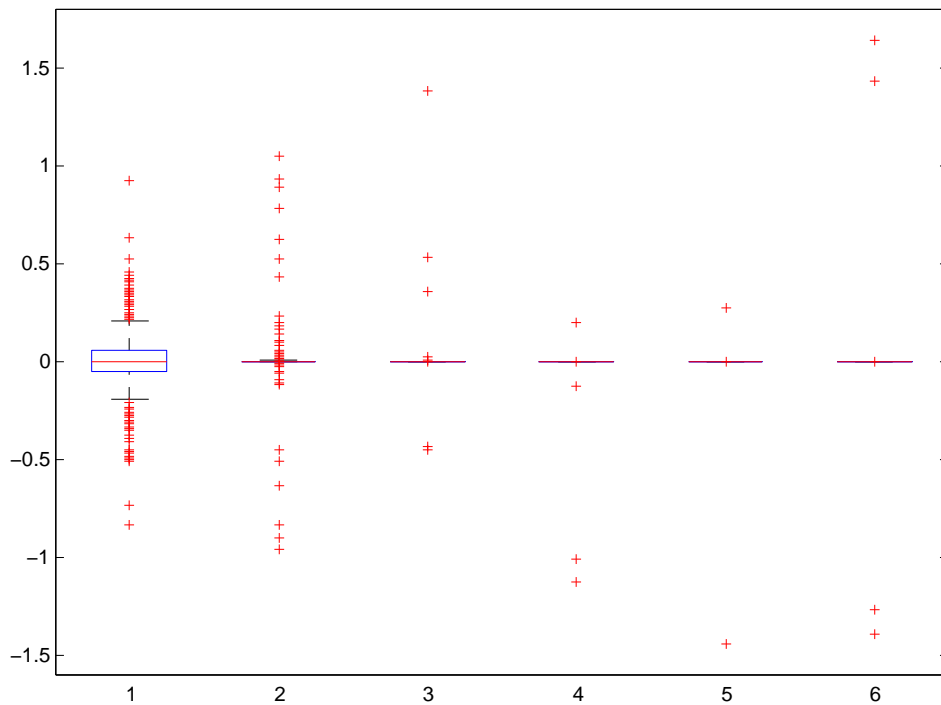


Figure 8: Side-by-side boxplots of posterior mean estimates of the columns of the factor loading matrix $\mathbf{\Lambda}_{:,1}$ (1), \dots , $\mathbf{\Lambda}_{:,6}$ (6), where $k = 6$ is the posterior mean estimate of the number of factors. The more these parameters are shrunk toward zero, the closer the model becomes to its “independent” version with $\mathbf{\Lambda} \equiv \mathbf{0}$.

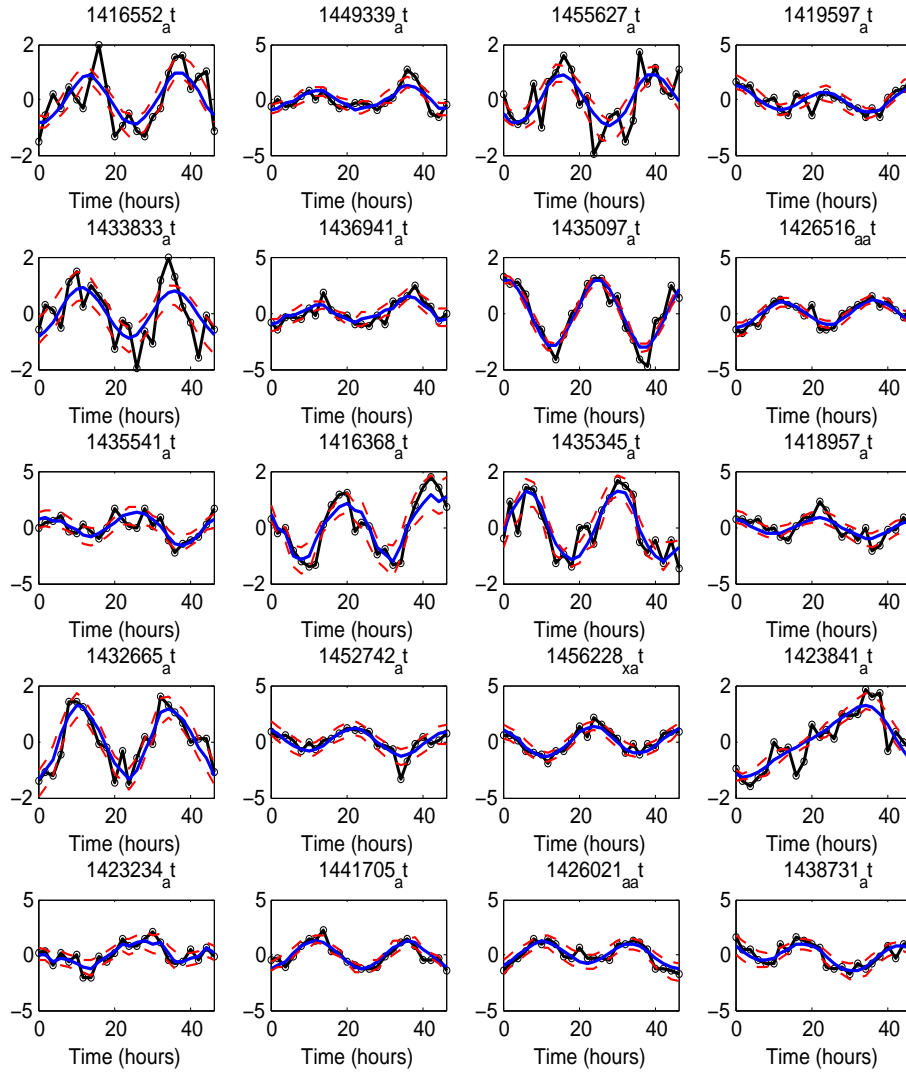


Figure 9: The top 20 probes in the mouse liver microarray dataset according to the posterior probability of being periodic from Equation (21). The black trajectory connects the true expression levels, the blue line represents the posterior mean, and red lines are the pointwise 95% credible intervals. The y -axis denotes the log-transformed and normalized expression levels.

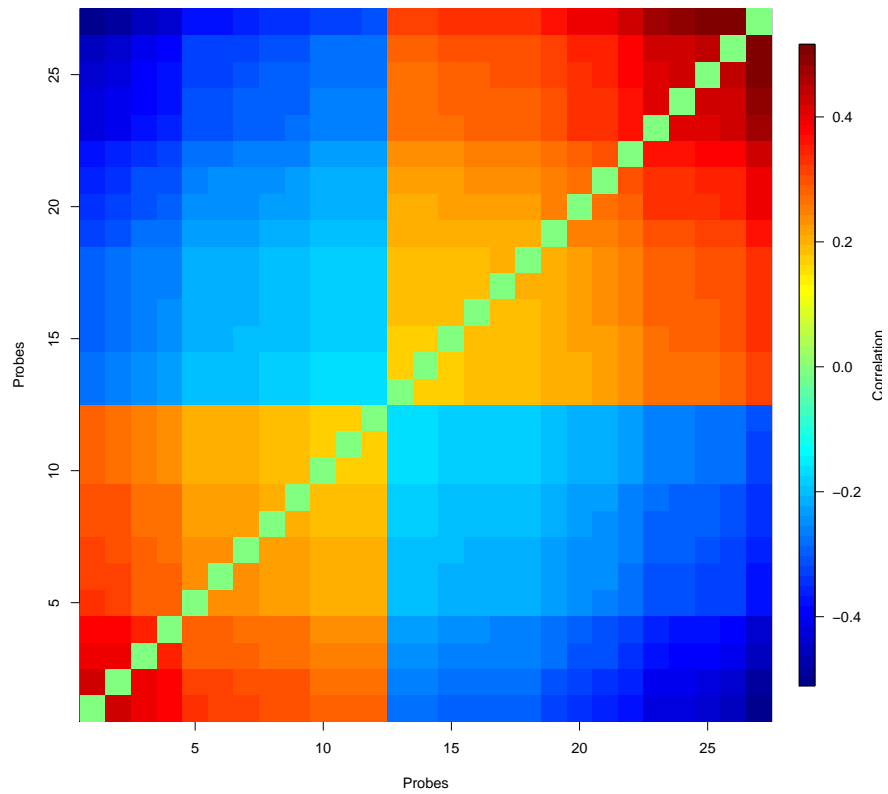


Figure 10: Correlation structure of the 27 proteins with strongest inferred correlation (of or above 0.30). To improve visibility, the diagonal of the correlation matrix was set to 0.

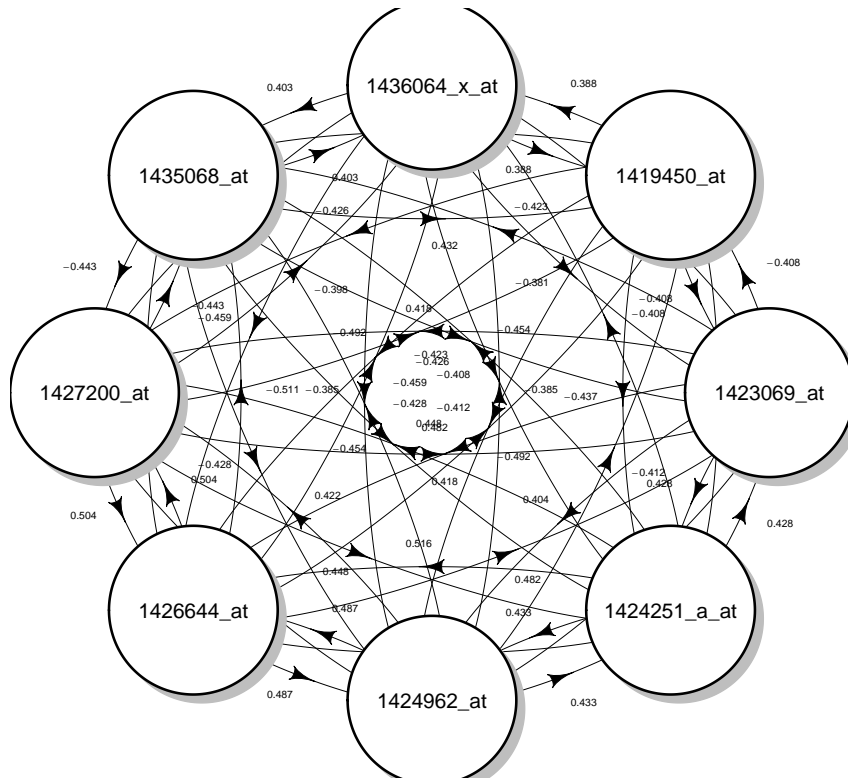


Figure 11: Network graph of probes with estimated correlation of or above 0.45 in absolute value.

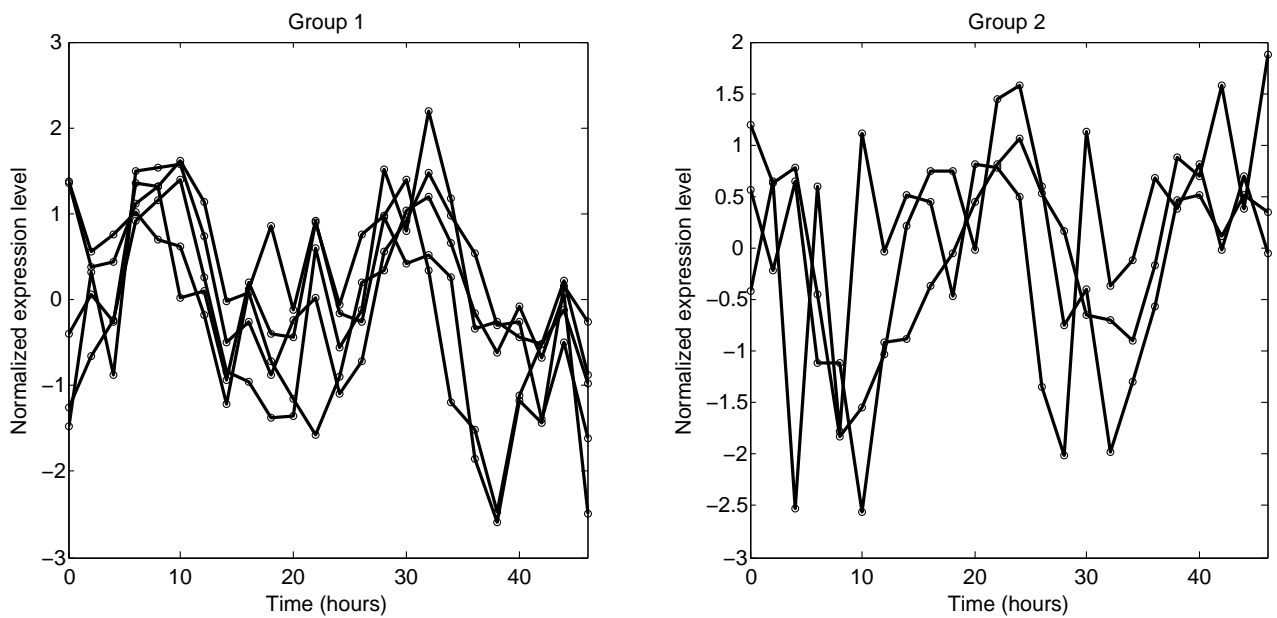


Figure 12: True trajectories of proteins with largest inferred correlations. These trajectories were obtained by linearly connecting the observed normalized expression levels. Group 1 includes probes 1423069 AT, 1424251 A AT, 1424962 AT, 1426644 AT, 1427200 AT; group 2 includes probes 1419450 AT, 1435068 AT, 1436064 X AT. Proteins within each group are positively correlated with each other, whereas correlation is negative across groups.

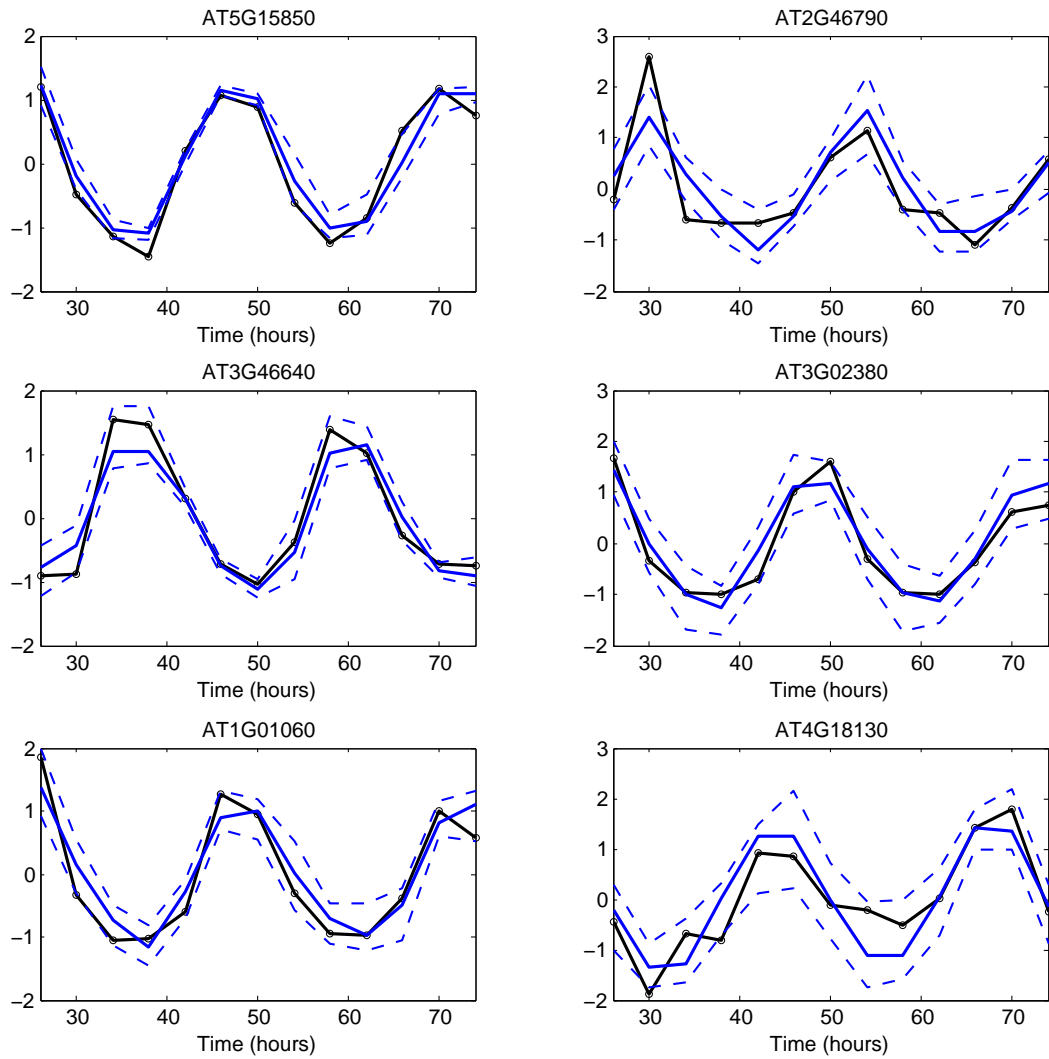


Figure 13: 6 well-known clock genes by biological knowledge of the *Arabidopsis* dataset that also rank top by posterior probability of being circadian from Equation (20). The black trajectory connects the true expression levels, the blue line represents the posterior mean, and dashed blue lines are the pointwise 95% credible intervals. The y -axis denotes the normalized expression levels.

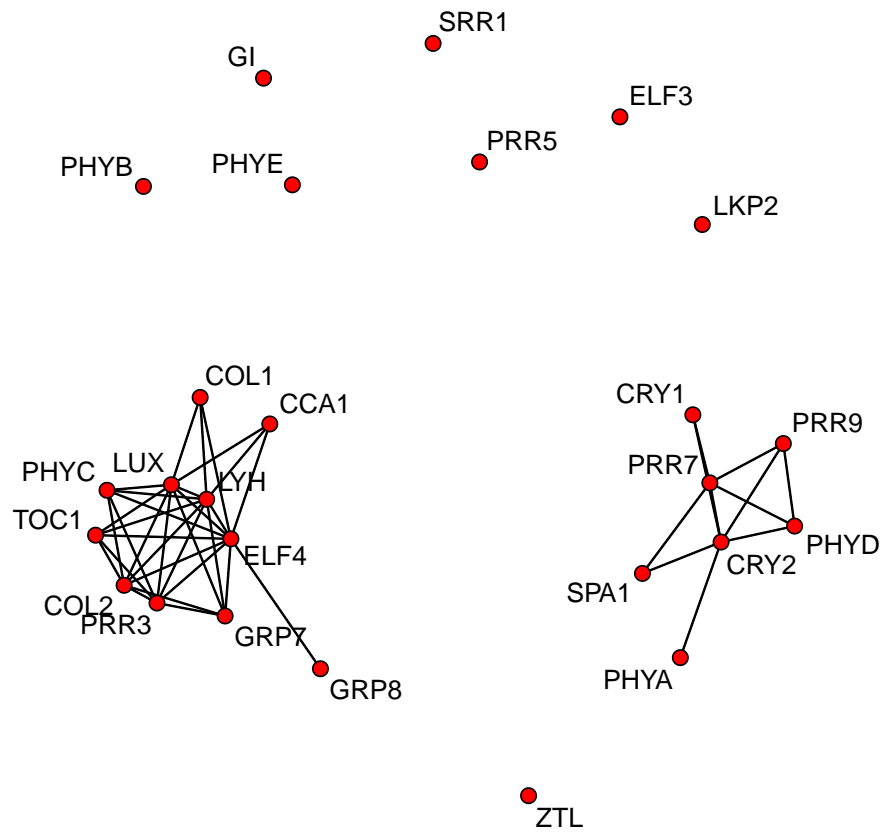


Figure 14: Network graph of the 26 known clock genes with lines connecting probes with inferred pairwise correlation of or above 0.05.